Organic nitrate chemistry and its implications for nitrogen budgets in an isoprene- and monoterpene-rich atmosphere: constraints from aircraft (SEAC[4]RS) and ground-based (SOAS) observations in the Southeast US

J. A. Fisher[1,2], D. J. Jacob[3,4], K. R. Travis[3], P. S. Kim[4], E. A. Marais[3], C. Chan Miller[4], K. Yu[3], L. Zhu[3], R. M. Yantosca[3], M. P. Sulprizio[3], J. Mao[5,6], P. O. Wennberg[7,8], J. D. Crounse[7], A. P. Teng[7], T. B. Nguyen[7,a], J. M. St. Clair[7,b], R. C. Cohen[9,10], P. Romer[9], B. A. Nault[10,c], P. J. Wooldridge[9], J. L. Jimenez[11,12], P. Campuzano-Jost[11,12], D. A. Day[11,12], W. Hu[11,12], P. B. Shepson[13,14], F. Xiong[13], D. R. Blake[15], A. H. Goldstein[16,17], P. K. Misztal[16], T. F. Hanisco[18], G. M. Wolfe[18,19], T. B. Ryerson[20], A. Wisthaler[21,22], and T. Mikoviny[21]

[1]Centre for Atmospheric Chemistry, School of Chemistry, University of Wollongong, Wollongong, NSW, Australia
[2]School of Earth and Environmental Sciences, University of Wollongong, Wollongong, NSW, Australia
[3]Harvard John A. Paulson School of Engineering and Applied Sciences, Harvard University, Cambridge, MA, USA
[4]Department of Earth and Planetary Sciences, Harvard University, Cambridge, MA, USA
[5]Program in Atmospheric and Oceanic Sciences, Princeton University, Princeton, NJ, USA
[6]Geophysical Fluid Dynamics Laboratory/National Oceanic and Atmospheric Administration, Princeton, NJ, USA
[7]Division of Geological and Planetary Sciences, California Institute of Technology, Pasadena, CA, USA
[8]Division of Engineering and Applied Science, California Institute of Technology, Pasadena, CA, USA
[9]Department of Chemistry, University of California at Berkeley, Berkeley, CA, USA
[10]Department of Earth and Planetary Science, University of California at Berkeley, Berkeley, CA, USA
[11]Department of Chemistry and Biochemistry, University of Colorado, Boulder, CO, USA
[12]Cooperative Institute for Research in Environmental Sciences, University of Colorado, Boulder, CO, USA
[13]Department of Chemistry, Purdue University, West Lafayette, IN, USA
[14]Department of Earth, Atmospheric and Planetary Sciences, Purdue University, West Lafayette, IN, USA
[15]Department of Chemistry, University of California Irvine, Irvine, CA, USA
[16]Department of Environmental Science, Policy, and Management, University of California at Berkeley, Berkeley, CA, USA
[17]Department of Civil and Environmental Engineering, University of California at Berkeley, Berkeley, CA, USA
[18]Atmospheric Chemistry and Dynamics Laboratory, NASA Goddard Space Flight Center, Greenbelt, MD, USA
[19]Joint Center for Earth Systems Technology, University of Maryland Baltimore County, Baltimore, MD, USA
[20]Chemical Sciences Division, Earth System Research Lab, National Oceanic and Atmospheric Administration, Boulder, CO, USA
[21]Department of Chemistry, University of Oslo, Oslo, Norway
[22]Institute for Ion Physics and Applied Physics, University of Innsbruck, Innsbruck, Austria
[a]Now at Department of Environmental Toxicology, University of California at Davis, Davis, CA, USA
[b]Now at Atmospheric Chemistry and Dynamics Laboratory, NASA Goddard Space Flight Center, Greenbelt, MD, USA and Joint Center for Earth Systems Technology, University of Maryland Baltimore County, Baltimore, MD, USA
[c]Now at Department of Chemistry and Biochemistry and Cooperative Institute for Research in Environmental Sciences, University of Colorado, Boulder, CO, USA

Correspondence to: J.A. Fisher (jennyf@uow.edu.au)

Abstract. Formation of organic nitrates ($RONO_2$) during oxidation of biogenic volatile organic compounds (BVOCs: isoprene, monoterpenes) is a significant loss pathway for atmospheric nitrogen oxide radicals (NO_x), but the chemistry of $RONO_2$ formation and degradation remains uncertain. Here we implement a new BVOC oxidation mechanism (including updated isoprene chemistry, new monoterpene chemistry, and particle uptake of $RONO_2$) in the GEOS-Chem global chemical transport model with $\sim 25 \times 25$ km^2 resolution over North America. We evaluate the model using aircraft (SEAC[4]RS) and ground-based (SOAS) observations of NO_x, BVOCs, and $RONO_2$ from the Southeast US in summer 2013. The updated simulation successfully reproduces the concentrations of individual gas- and particle-phase $RONO_2$ species measured during the campaigns. Gas-phase isoprene nitrates account for 25-50% of observed $RONO_2$ in surface air, and we find that another 10% is contributed by gas-phase monoterpene nitrates. Observations in the free troposphere show an important contribution from long-lived nitrates derived from anthropogenic VOCs. During both campaigns, at least 10% of observed boundary layer $RONO_2$ were in the particle phase. We find that aerosol uptake followed by hydrolysis to HNO_3 accounts for 60% of simulated gas-phase $RONO_2$ loss in the boundary layer. Other losses are 20% by photolysis to recycle NO_x and 15% by dry deposition. $RONO_2$ production accounts for 20% of the net regional NO_x sink in the Southeast US in summer, limited by the spatial segregation between BVOC and NO_x emissions. This segregation implies that $RONO_2$ production will remain a minor sink for NO_x in the Southeast US in the future even as NO_x emissions continue to decline.

1 Introduction

Nitrogen oxide radicals ($NO_x \equiv NO + NO_2$) are critical in controlling tropospheric ozone production (Monks et al., 2015, and references therein) and influencing aerosol formation (Rollins et al., 2012; Ayres et al., 2015; Xu et al., 2015), with indirect impacts on atmospheric oxidation capacity, air quality, climate forcing, and ecosystem health. The ability of NO_x to influence ozone and aerosol budgets is tied to its atmospheric fate. In continental regions, a significant loss pathway for NO_x is reaction with peroxy radicals derived from biogenic volatile organic compounds (BVOCs) to form organic nitrates (Liang et al., 1998; Browne and Cohen, 2012). NO_x loss to organic nitrate formation is predicted to become increasingly important as NO_x abundance declines (Browne and Cohen, 2012), as has occurred in the US over the past two decades (Hidy et al., 2014; Simon et al., 2015). Despite this increasing influence on the NO_x budget, the chemistry of organic nitrates remains the subject of debate, with key uncertainties surrounding the organic nitrate yield from BVOC oxidation, the recycling of NO_x from organic nitrate degradation, and the role of organic nitrates in secondary organic aerosol formation (Paulot et al., 2012; Perring et al., 2013). Two campaigns in the Southeast US in summer 2013 provided datasets of unprecedented chemical detail for addressing these uncertainties: the airborne NASA SEAC[4]RS (Studies of Emissions and Atmospheric Composition, Clouds, and Climate Coupling by Regional Surveys; Toon et al., 2016) and the ground-based SOAS (Southern Oxidants and Aerosols Study). Here we use a $\sim 25 \times 25$ km^2 resolution 3-D chemical transport model (GEOS-Chem) to interpret organic nitrate observations from both campaigns, with focus on their impacts on atmospheric nitrogen (N) budgets.

Nitrogen oxides are emitted from natural and anthropogenic sources primarily as NO, which rapidly achieves steady state with NO_2. Globally, the dominant loss pathway for NO_x is reaction with the hydroxyl radical (OH) to form nitric acid (HNO_3).

In the presence of VOCs, NO_x can also be lost by reaction with organic peroxy radicals (RO_2) to form peroxy nitrates (RO_2NO_2) and alkyl and multifunctional nitrates ($RONO_2$) (O'Brien et al., 1995). Their daytime formation temporarily sequesters NO_x, facilitating its export to more remote environments (Horowitz et al., 1998; Paulot et al., 2012; Mao et al., 2013). RO_2NO_2 species are thermally unstable at boundary layer temperatures and decompose back to NO_x on a time scale

5   of minutes, except for the longer-lived peroxyacylnitrates (PANs) (Singh and Hanst, 1981). $RONO_2$ species can dominate NO_x loss when BVOC emissions are high and NO_x emissions are low (Browne and Cohen, 2012; Paulot et al., 2012; Browne et al., 2014) and may be more efficient for reactive N export than PANs (Mao et al., 2013). The amount of NO_x sequestered by $RONO_2$ depends on the interplay between BVOC and NO_x emissions, the $RONO_2$ yield from BVOC oxidation, and the eventual $RONO_2$ fate.

10   $RONO_2$ chemistry and impacts are illustrated schematically in Fig. 1, starting from reaction of NO_x with BVOCs (mainly isoprene and monoterpenes) to form $RONO_2$. The $RONO_2$ yield (α) from isoprene oxidation by OH has been inferred from laboratory and field experiments to be 4-15% (Tuazon and Atkinson, 1990; Chen et al., 1998; Sprengnether et al., 2002; Patchen et al., 2007; Perring et al., 2009a; Paulot et al., 2009; Nguyen et al., 2014; Xiong et al., 2015). Models have shown nearly this full range of yields to be compatible with $RONO_2$ observations, depending on the chemical mechanism assumed. For example,

15   two models using different isoprene reaction schemes both successfully reproduced observations from a 2004 aircraft campaign (ICARTT) - one assuming a 4% molar yield (Horowitz et al., 2007) and the other assuming an 11.7% molar yield (Mao et al., 2013). The $RONO_2$ yield from monoterpene oxidation by OH is even more uncertain. Laboratory measurements exist only for α-pinene, and these show divergent results: 26% (Rindelaub et al., 2015), 18% (Nozière et al., 1999), and 1% (Aschmann et al., 2002, a lower limit due to significant wall losses). $RONO_2$ yields remain a significant uncertainty in BVOC oxidation

20   schemes, with implications for their impacts on NO_x sequestration.

The fate of $RONO_2$ is of central importance in determining whether sequestered NO_x is returned to the atmosphere or removed irreversibly. Many first generation $RONO_2$ (i.e., those formed from NO reaction with BVOC-derived peroxy radicals) have a short lifetime against further oxidation to form a suite of second generation $RONO_2$ (Beaver et al., 2012; Mao et al., 2013; Browne et al., 2014), especially if they are produced from di-olefins such as isoprene or limonene. Laboratory studies

25   indicate little NO_x release during this process (Lee et al., 2014); however, NO_x can be recycled by subsequent oxidation and photolysis of second generation species (Müller et al., 2014). Estimates of the NO_x recycling efficiency, defined as the mean molar percentage of $RONO_2$ loss that releases NO_x, range from <5% to >50% for isoprene nitrates (INs) (Horowitz et al., 2007; Paulot et al., 2009), and best estimates depend on assumptions about the IN yield (Perring et al., 2009a). NO_x recycling efficiencies from monoterpene nitrates (MTNs) have not been observed experimentally, but model sensitivity studies have

30   shown a 14% difference in boundary layer NO_x between scenarios assuming 0% versus 100% recycling (assuming an initial 18% MTN yield, Browne et al., 2014). Uncertainty in the NO_x recycling efficiency has a bigger impact on simulation of NO_x and ozone than uncertainty in the $RONO_2$ yield (Xie et al., 2013).

Organic nitrates are more functionalized and less volatile than their BVOC precursors and are therefore more likely to partition to the particle phase. In the Southeast US, Xu et al. (2015) recently showed that particulate $RONO_2$ ($pRONO_2$)

35   make an important contribution to total organic aerosol (5-12%), consistent with in situ observations from other environments

(Brown et al., 2009, 2013; Fry et al., 2013; Rollins et al., 2012, 2013). Chamber experiments have shown high mass yields of aerosol from NO_3-initiated oxidation of isoprene (15-25%; Ng et al., 2008; Rollins et al., 2009) and some monoterpenes (33-65%; Fry et al., 2014). There is evidence that $RONO_2$ from OH-initiated oxidation also form aerosol, although with lower yields, possibly via multi-functionalized oxidation products (Kim et al., 2012; Lin et al., 2012; Rollins et al., 2012; Lee et al., 2014). $pRONO_2$ are removed either by deposition or by hydrolysis to form HNO_3 (Jacobs et al., 2014; Rindelaub et al., 2015). Both losses augment N deposition to ecosystems (Lockwood et al., 2008). Aerosol partitioning competes with photochemistry as a loss for gas-phase $RONO_2$ with impacts for NO_x recycling. Partitioning also competes with gas-phase deposition, and because lifetimes against deposition are much longer for organic aerosols than for gas-phase precursors (Wainwright et al., 2012; Knote et al., 2015), this process may shift the enhanced N deposition associated with $RONO_2$ (Zhang et al., 2012; Nguyen et al., 2015) to ecosystems further downwind of sources.

The 2013 SEAC^{4}RS and SOAS campaigns provide a unique resource for evaluating the impact of BVOC-derived organic nitrates on atmospheric NO_x. Both campaigns provided datasets of unprecedented chemical detail, including isoprene, monoterpenes, total and particle-phase $RONO_2$, and speciated INs; during SOAS these were further augmented by measurements of MTNs. Continuous measurements from the SOAS ground site provide high temporal resolution and constraints on diurnal variability (e.g., Nguyen et al., 2015; Xiong et al., 2015). These are complemented by extensive boundary layer profiling across a range of chemical environments from the SEAC^{4}RS airborne measurements (Toon et al., 2016). Combined, the campaigns covered the summer period when BVOC emissions in the Southeast US are at a maximum (Palmer et al., 2006). These data offer new constraints for testing models of organic nitrate chemistry, with implications for our understanding of NO_x, ozone, and aerosol budgets in BVOC-dominated environments worldwide.

We examine here the impact of BVOC oxidation on atmospheric NO_x, using the 2013 campaign data combined with the GEOS-Chem model. The version of GEOS-Chem used in this work represents a significant advance over previous studies, with higher spatial resolution ($\sim25\times25$ km^2) that better captures the spatial segregation of BVOC and NO_x emissions (Yu et al., 2016); updated isoprene nitrate chemistry incorporating new experimental and theoretical findings (e.g., Lee et al., 2014; Müller et al., 2014; Peeters et al., 2014; Xiong et al., 2015); addition of monoterpene nitrate chemistry (Browne et al., 2014; Pye et al., 2015); and consideration of particle uptake of gas-phase isoprene and monoterpene nitrates. We first evaluate the updated GEOS-Chem simulation using SOAS and SEAC^{4}RS observations of BVOCs, organic nitrates, and related species. We then use GEOS-Chem to quantify the fates of BVOC-derived organic nitrates in the Southeast US. Finally, we investigate the impacts of organic nitrate formation on the NO_x budget.

2   Updates to GEOS-Chem simulation of organic nitrates

We use a new high resolution version of the GEOS-Chem CTM (www.geos-chem.org) v9-02, driven by assimilated meteorology from the NASA Global Modeling and Assimilation Office (GMAO) Goddard Earth Observing System Forward Processing (GEOS-FP) product. The model is run in a nested configuration (Wang et al., 2004), with native GEOS-FP horizontal resolution of 0.25° latitude by 0.3125° longitude over North America (130-60°W, 9.75-60°N). Boundary conditions are provided

from a $4° \times 5°$ global simulation, also using GEOS-Chem. The native GEOS-FP product includes 72 vertical layers of which $\sim$38 are in the troposphere. Temporal resolution of GEOS-FP is hourly for surface variables and 3-hourly for all others. Our simulations use a time step of 5 minutes for transport and 10 minutes for emissions and chemistry.

GEOS-Chem has been applied previously to simulation of organic nitrates in the Southeast US (e.g., Fiore et al., 2005; Zhang et al., 2011; Mao et al., 2013). Mao et al. (2013) recently updated the GEOS-Chem isoprene oxidation mechanism to include explicit production and loss of a suite of second generation isoprene nitrates and nighttime oxidation by nitrate radicals. While their updated simulation showed good agreement with aircraft observations from the 2004 ICARTT campaign over the eastern US, we find that the more detailed chemical payloads available during SOAS and SEAC[4]RS highlight deficiencies in that mechanism, resulting in large model biases in $RONO_2$.

A major component of this work is modification of the organic nitrate simulation in GEOS-Chem. Our focus here is on the BVOC-derived nitrates for which field measurements are newly available. GEOS-Chem simulation of PANs was recently updated by Fischer et al. (2014) and is not discussed here. Our improvements to the $RONO_2$ simulation are detailed below and include updates to isoprene oxidation chemistry, addition of monoterpene oxidation chemistry, and inclusion of aerosol uptake of $RONO_2$ followed by particle-phase hydrolysis. Other updates from GEOS-Chem v9-02 and comparison to Southeast US observations are presented in several companion papers. Kim et al. (2015) describe the aerosol simulation and Travis et al. (2016) the gas-phase oxidant chemistry. Constraints on isoprene emissions from satellite formaldehyde observations are described by Zhu et al. (2016). The low-NO_x isoprene oxidation pathway and implications for organic aerosols are described by Marais et al. (2016). Finally, Yu et al. (2016) evaluate the impact of model resolution and spatial segregation of NO_x and BVOC emissions on isoprene oxidation. Our simulation is identical to that used in Travis et al. (2016), Yu et al. (2016), and Zhu et al. (2016).

2.1 Isoprene oxidation chemical mechanism

The basic structure of the GEOS-Chem isoprene oxidation mechanism is described by Mao et al. (2013), with updates to low-NO_x pathways described and validated by Travis et al. (2016). All updates to the isoprene oxidation mechanism are provided in Travis et al. (2016) Tables S1 and S2. Figure 2 shows our updated implementation of OH-initiated isoprene oxidation in the presence of NO_x leading to isoprene nitrate (IN) formation. Isoprene oxidation by OH produces isoprene peroxy radicals ($ISOPO_2$) in either β- or δ-hydroxy peroxy configurations depending on the location of OH addition. In the presence of NO_x, $ISOPO_2$ reacts with NO to either produce NO_2 (the dominant fate; Perring et al., 2013) or form INs, with the yield of INs (α) defined as the branching ratio between these two channels. Early laboratory measurements of α suggested an IN yield between 4.4 and 12% (Tuazon and Atkinson, 1990; Chen et al., 1998; Sprengnether et al., 2002; Patchen et al., 2007; Paulot et al., 2009; Lockwood et al., 2010). More recent experiments indicate continuing uncertainty in α, with a measured yield of $\alpha = 9 \pm 4\%$ from the Purdue Chemical Ionization Mass Spectrometer (CIMS; Xiong et al., 2015) and $\alpha = 13 \pm 2\%$ from the Caltech CF_3O^- Time-of-Flight CIMS (CIT-ToF-CIMS; Teng et al., in preparation), despite excellent agreement during calibrated intercomparison exercises using one isoprene nitrate isomer (4,3 ISOPN). The sensitivity of the CIT-ToF-CIMS is similar for all isomers of ISOPN (Lee et al., 2014), while the Purdue instrument is less sensitive to the major isomer

(1,2 ISOPN) (Xiong et al., 2015). Here, we use a first generation IN yield of $\alpha = 9\%$, which we find provides a reasonable simulation of the SOAS observations and is also consistent with the SOAS box model simulations of Xiong et al. (2015). We discuss the model sensitivity to the choice of α in Sect. 3.

For the oxidation of isoprene by OH, the mechanism described in Mao et al. (2013) assumed a first generation IN composition of 40% β-hydroxyl INs (β-ISOPN) and 60% δ-hydroxyl INs (δ-ISOPN). However, new theoretical constraints show that under atmospheric conditions, δ-channel peroxy radicals are only a small fraction of the total due to fast redissociation of peroxy radicals that fosters interconversion between isomers and tends towards an equilibrium population with more than 95% β-isomers (Peeters et al., 2014). Using a simplified box model based on the extended Leuven Isoprene Mechanism LIM1, we found δ-isomers were 4-8% of the total peroxy pool in representative Southeast US boundary layer conditions (temperature $\sim$295-300 K, ISOPO$_2$ lifetime $\sim$20-60 seconds). In what follows, we use an IN distribution of 90% β-ISOPN and 10% δ-ISOPN. Our box modeling suggests 10% is an upper limit for the δ-ISOPN pool; however, we maintain this value as it allows improved simulation of species with predominantly δ-pathway origins, including glyoxal and the second generation INs propanone nitrate (PROPNN) and ethanal nitrate (ETHLN).

First generation ISOPN isomers formed via OH oxidation of isoprene have a short photochemical lifetime against atmospheric oxidation (Paulot et al., 2009; Lockwood et al., 2010; Lee et al., 2014). Here we use updated reaction rate constants and products from Lee et al. (2014) that increase the β-ISOPN+OH reaction by roughly a factor of two and decrease ozonolysis by three orders of magnitude (relative to the previous mechanism based on Lockwood et al., 2010; Paulot et al., 2009). Changes in δ-ISOPN reaction rate constants are more modest but in the same direction. For both isomers, reaction with OH forms a peroxy radical (ISOPNO$_2$) along with a small (10%) yield of isoprene epoxy diols (Jacobs et al., 2014). Rate constants and products of the subsequent oxidation of ISOPNO$_2$ to form a suite of second generation INs follow the Lee et al. (2014) mechanism. We explicitly simulate methylvinylketone nitrate (MVKN) and methacrolein nitrate (MACRN), which are primarily from the β-pathway; PROPNN and ETHLN, which are primarily from the δ-pathway (and NO$_3$-initiated oxidation); and C$_5$ dihydroxy dinitrate (DHDN), formed from both isomers (Lee et al., 2014).

Isoprene reaction with NO$_3$ is the dominant isoprene sink at night and can also be significant during the day (Ayres et al., 2015), producing INs with high yield (Perring et al., 2009b; Rollins et al., 2009). This reaction can account for more than 20% of isoprene loss in some environments (Brown et al., 2009) and may explain 40-50% of total RONO$_2$ in the Southeast (Mao et al., 2013; Xie et al., 2013). The mechanism used here is identical to that described by Mao et al. (2013). Reaction of isoprene with NO$_3$ forms a nitrooxy peroxy radical (INO$_2$). Subsequent reaction of INO$_2$ with NO, NO$_3$, itself, or other peroxy radicals forms a first generation C$_5$ carbonyl nitrate (ISN1) with 70% yield, while reaction with HO$_2$ forms a C$_5$ nitrooxy hydroperoxide (INPN) with 100% yield. In this simplified scheme, we do not distinguish between β- and δ- isomers for ISN1 and INPN, nor do we include the C$_5$ hydroxy nitrate species recently identified in chamber experiments (Schwantes et al., 2015). Mao et al. (2013) lumped all second generation nitrates derived from ISN1 and INPN into a single species (R$_4$N$_2$), but here we assume that the lumped species is PROPNN on the basis of recent chamber experiments that show PROPNN to be a high-yield photooxidation product of INs from NO$_3$-initiated oxidation (Schwantes et al., 2015). This effectively assumes

instantaneous conversion of INs to PROPNN, a simplification that results in a shift in the simulated diurnal cycle of PROPNN (see Sect. 3). We do not include here the nitrooxy hydroxyepoxide product recently identified by Schwantes et al. (2015).

Possible fates for second generation INs include further oxidation, photolysis, uptake to the aerosol phase followed by hydrolysis (Sect. 2.3), and removal via wet and dry deposition. Müller et al. (2014) show that photolysis is likely significantly faster than reaction with OH for carbonyl nitrates (e.g., MVKN, MACRN, ETHLN, PROPNN) due to enhanced absorption cross sections and high quantum yields caused by the proximity of the carbonyl group (a strongly absorbing chromophore) to the weakly-bound nitrate group. Here we increase the absorption cross sections of the carbonyl INs following the methodology of Müller et al. (2014, Sect. 2). Briefly, we first use the PROPNN cross section measured by Barnes et al. (1993) to calculate a wavelength-dependent cross section enhancement ratio (r_{nk}), defined as the ratio of the measured cross section to the sum of the IUPAC-recommended cross sections for associated monofunctional nitrates and ketones. We then calculate new cross sections for ETHLN, MVKN, and MACRN by multiplying r_{nk} by the sum of cross sections from appropriate monofunctional analogues (Table S5). The new cross sections are 5-15 times larger than in the original model, which used the IUPAC-recommended cross section of the monofunctional analogue tert-butyl nitrate for all carbonyl nitrates (Roberts and Fajer, 1989). For all species, we calculate photolysis rates assuming unity quantum yields, whereby the weak $O-NO_2$ bond dissociates upon a rearrangement after photon absorption to the carbonyl chromophore (Müller et al., 2014). Peak midday photolysis rates now range from $\sim 3 \times 10^{-5}\,\mathrm{s}^{-1}$ (PROPNN) to $\sim 3 \times 10^{-4}\,\mathrm{s}^{-1}$ (MACRN).

Removal by dry deposition has been updated based on new observations from the SOAS ground site. The dry deposition calculation is now constrained to match observed deposition velocities for ISOPN, MVKN, MACRN, and PROPNN (Nguyen et al., 2015; Travis et al., 2016), with all other $RONO_2$ deposition velocities scaled to that of ISOPN. Wet scavenging of gases is described in Amos et al. (2012) and has been modified here to use the same Henry's Law coefficients as for dry deposition. Aerosol partitioning is described in Sect. 2.3 below.

2.2 Monoterpene oxidation chemical mechanism

Monoterpene chemistry is not included in the standard GEOS-Chem gas-phase chemical mechanism. Here we implement a monoterpene nitrate scheme developed by Browne et al. (2014) that was built on the RACM2 chemical mechanism (Goliff et al., 2013) and evaluated using aircraft observations over the Canadian boreal forest (Browne et al., 2014). Our implementation is summarized in Fig. 3 and described briefly below, with the full mechanism available in the Supplement (Tables S1-S3) and at http://wiki.seas.harvard.edu/geos-chem/index.php/Monoterpene_nitrate_scheme. We include two lumped monoterpene tracers: API representing monoterpenes with one double bond (α-pinene, β-pinene, sabinene, and Δ-3-carene) and LIM representing monoterpenes with two double bonds (limonene, myrcene, and ocimene). Combined, these species account for roughly 90% of all monoterpene emissions (Guenther et al., 2012), and we neglect other terpenes here. During the day, LIM and API are oxidized by OH to form peroxy radicals. Subsequent reaction with NO forms first generation monoterpene nitrates with a yield of 18% (Nozière et al., 1999). These can be either saturated (MONITS) or unsaturated (MONITU), with precursor-dependent partitioning as shown in Fig. 3. For all subsequent discussion, we refer to their sum MONIT = MONITU + MONITS.

At night, both LIM and API react with NO_3 to form a nitrooxy peroxy radical that either decomposes to release NO_2 or retains the nitrate functionality to form MONIT. The branching ratio between these two fates is 50% nitrate-retaining for LIM + NO_3 (Fry et al., 2014) and 10% nitrate-retaining for API + NO_3 (Browne et al., 2014). The 10% nitrate yield from API + NO_3 is on the low end of the observed range (Fry et al., 2014), so simulated pinene-derived MONIT should be considered a lower bound. In Browne et al. (2014), the API + NO_3 reaction used the α-pinene + NO_3 rate constant from the Master Chemical Mechanims (MCMv3.2). We have updated this rate constant to $k_{API+NO_3} = 8.33 \times 10^{-13} e^{490/T}$, a rough average of the MCMv3.3 α- and β-pinene values, as API comprises both α- and β-pinenes (the dominant API components, present in roughly equal amounts during both SEAC[4]RS and SOAS). API and LIM also react with O_3, but this reaction does not lead to $RONO_2$ formation.

We do not distinguish between OH-derived and NO_3-derived MTN species. MONIT are subject to removal via wet and dry scavenging, aerosol uptake, photolysis, ozonolysis (MONITU only) and oxidation by OH. Here, we also add MONIT reaction with NO_3 with the same rate constant as used for nighttime isoprene nitrates. The products of MONIT oxidation are currently unknown; here we follow Browne et al. (2014) and assume oxidation produces a second generation monoterpene nitrate (HONIT) that undergoes dry deposition, photolysis, and oxidative loss. In our simulation, HONIT is also removed via aerosol uptake (Sect. 2.3).

2.3 Aerosol partitioning of $RONO_2$

Evidence from laboratory and field studies suggests aerosol uptake is a potentially significant loss pathway for gas-phase $RONO_2$ (e.g., Day et al., 2010; Rollins et al., 2010; Darer et al., 2011; Fry et al., 2013, 2014). In particular, BVOC oxidation by NO_3 radicals has been shown to result in high organic aerosol yields (Ng et al., 2008; Fry et al., 2009; Rollins et al., 2012). Recent work from SOAS highlighted the role of the monoterpenes + NO_3 reaction, with an estimated 23-44% yield of organic nitrate aerosol (Ayres et al., 2015) that can explain roughly half of nighttime secondary organic aerosol production (Xu et al., 2014). Isoprene + NO_3 results in smaller but still significant yields; Xu et al. (2014) estimate that isoprene was responsible for 20% of nighttime NO_3-derived organic aerosol observed during SOAS. Organic nitrate aerosol yields from daytime oxidation by OH are lower but non-negligible. At Bakersfield, for example, Rollins et al. (2013) found 21% of $RONO_2$ partitioned to the aerosol phase during the day, and that these could explain 5% of the total daytime organic aerosol mass.

Aerosol partitioning of $RONO_2$ has not previously been considered in GEOS-Chem. Here we add this process using a reactive uptake coefficient (γ) parameterization. Our parameterization was designed to provide a necessary sink for gas-phase $RONO_2$ species (overestimated in earlier iterations of our model), and therefore makes a number of simplifying assumptions. In particular, we do not allow $pRONO_2$ to re-partition to the gas phase (likely to impact the more volatile isoprene-derived nitrates), and uptake coefficients are defined to fit the measurements of gas-phase species. More accurate simulation of organic nitrate aerosols would require additional updates that take into account vapor pressure differences between species (as done recently by Pye et al., 2015) and incorporate new findings from SOAS (Ayres et al., 2015; Lee et al., 2016). For our simulation, we apply reactive uptake to all BVOC-derived $RONO_2$ except PROPNN and ETHLN, which lack hydroxyl groups and are therefore expected to be significantly less soluble. We assume an uptake coefficient of γ=0.005 for isoprene nitrates (from both

daytime and nighttime chemistry) and $\gamma=0.01$ for all monoterpene nitrates (Table S4). Our isoprene nitrate uptake coefficient is in the middle of the range predicted by Marais et al. (2016) using a mechanistic formulation, and is a factor of 4 lower than the upper limit for ISOPN inferred by Wolfe et al. (2015) using SEAC[4]RS flux measurements. Although simplified, we find this parameterization provides a reasonable fit to the SEAC[4]RS and SOAS observations of individual gas-phase $RONO_2$ species measured by the CIT-ToF-CIMS and total $pRONO_2$ measured by an Aerosol Mass Spectrometer (AMS) (see Sect. 3 and 4).

After partitioning to the aerosol, laboratory experiments have shown that $pRONO_2$ can hydrolyze to form alcohols and nitric acid via $pRONO_2 + H_2O \rightarrow ROH + HNO_3$. Some $pRONO_2$ species hydrolyze rapidly under atmospherically-relevant conditions, while others are stable against hydrolysis over timescales significantly longer than the organic aerosol lifetime against deposition (Darer et al., 2011; Hu et al., 2011; Liu et al., 2012; Jacobs et al., 2014; Rindelaub et al., 2015). Lifetimes against hydrolysis inferred from bulk aqueous and reaction chamber studies range widely from minutes (Darer et al., 2011; Rindelaub et al., 2015) to a few hours (Liu et al., 2012; Lee et al., 2016) to nearly a day (Jacobs et al., 2014). Here we apply a bulk lifetime against hydrolysis for the entire population of $pRONO_2$ (similar to Pye et al., 2015). In other words, our implementation of aerosol partitioning involves a two-step process of (1) uptake of gas-phase $RONO_2$ to form a simplified non-volatile $pRONO_2$ species, with rate determined by γ, followed by (2) hydrolysis of the simplified $pRONO_2$ species to form HNO_3, with rate determined by the lifetime against hydrolysis. These steps are de-coupled, and we do not include any dependence of γ on the hydrolysis rate (unlike the more detailed formulation of Marais et al. (2016)). In subsequent sections, we compare the simplified $pRONO_2$ formed as an intermediate during this process to total $pRONO_2$ derived from observations. The assumption of a single hydrolysis lifetime overestimates the loss rate of non-tertiary nitrates (Darer et al., 2011; Hu et al., 2011) and may lead to model bias in total $pRONO_2$, particularly in the free troposphere where the longer-lived species would be more prevalent (see Sect. 4).

We assume here a bulk lifetime against hydrolysis of 1 h, which we found in preliminary simulations to provide a better simulation of $pRONO_2$ than longer lifetimes. Our 1 h bulk hydrolysis lifetime is shorter than the 2-4 h lifetime found in recent analysis of SOAS data and laboratory experiments (Boyd et al., 2015; Lee et al., 2016; Pye et al., 2015) - likely reflecting the simplifying assumptions of our uptake parameterization. In any case, the choice of hydrolysis lifetime does not affect the concentration of gas-phase $RONO_2$ species (because $pRONO_2$ cannot re-partition to the gas phase in the model), and we find this value provides a reasonable match to AMS measurements of total $pRONO_2$ at the surface during SOAS and SEAC[4]RS (see Sect. 3 and 4). Impacts on HNO_3 are minor: compared to a simulation without hydrolysis, our simulation with a 1 h lifetime against hydrolysis increased boundary layer HNO_3 by 20 ppt, or 2.4%.

3   BVOCs and organic nitrates in the Southeast US

We evaluate the updated GEOS-Chem simulation using Southeast US measurements of isoprene, monoterpenes, and a suite of oxidation products from two field campaigns in summer 2013. SEAC[4]RS was a NASA aircraft campaign that took place in August-September 2013 (Toon et al., 2016). All observations discussed in this work were taken onboard the NASA DC-8 (data doi: 10.5067/Aircraft/SEAC[4]RS/Aerosol-TraceGas-Cloud), which was based in Houston, Texas with an $\sim$8-hour flight range.

SOAS was a ground-based campaign that took place in June-July 2013 at the Centreville monitoring site near Brent, Alabama (32.903°N, 87.250°W).

3.1 Isoprene and monoterpenes

Understanding BVOC sources and chemistry was a primary goal of SEAC[4]RS, resulting in a large number of boundary layer flights over regions of enhanced biogenic emissions (Kim et al., 2015). Isoprene and monoterpene distributions in Southeast US surface air (80-94.5°W, 29.5-40°N, and below 1 km) measured by PTR-MS are shown in Fig. 4, and their campaign-median vertical profiles are shown in Fig. 5(b,c). Whole Air Sampler (WAS) measurements of isoprene and α-pinene + β-pinene (Fig. S1) are similar, but with more limited sampling than the PTR-MS. All observations have been averaged to the spatial and temporal resolution of the model.

The SOAS site is located at the edge of a mixed coniferous and deciduous forest (Nguyen et al., 2015). SOAS observations of isoprene and monoterpenes, measured by PTR-ToF-MS and averaged to hourly mean values, are shown in Fig. 6. Both species display a clear diurnal cycle with peak isoprene during day, reflecting the light- and temperature-dependent source, and peak monoterpenes at night. For monoterpenes, the figure also shows the sum of α-pinene + β-pinene as measured by 2D-GC-FID, which indicates that these are the dominant monoterpenes.

Figures 4, 5, and 6 compare observed BVOCs from both campaigns to the GEOS-Chem simulation, sampled to match the observations. Similar figures for NO_x can be found in Travis et al. (2016) and in Fig. S2. Model bias relative to observations is quantified using the normalized mean bias $\text{NMB} = 100\% \times [\sum_i (M_i - O_i) / \sum_i (O_i)]$, where O_i and M_i are the observed and modeled values and the summation is over all hours (SOAS) or unique gridbox-timestep combinations along the flight tracks (SEAC[4]RS). BVOC emissions are from MEGANv2.1 (Guenther et al., 2012) and have been decreased by 15% for isoprene and doubled for monoterpenes to better match aircraft (isoprene, monoterpene) and satellite (formaldehyde) observations (Kim et al., 2015; Zhu et al., 2016). With these scalings applied, simulated surface isoprene and monoterpenes overestimate somewhat the SEAC[4]RS data (Fig. 4, mainly due to a few simulated high-BVOC events), but the medians are well within the observed variability (Fig. 5). Model high bias above 500 m is likely caused by excessive vertical mixing through the simulated boundary layer (Travis et al., 2016). Relative to the SOAS data, simulated monoterpenes are biased low by a factor of two, while isoprene falls within the interquartile range of the measurements. The opposite sign of the SOAS monoterpene bias relative to the more spatially representative SEAC[4]RS data suggests a low bias in MEGANv2.1 monoterpene emissions that is unique to the Centreville gridbox; errors in vertical mixing may also contribute. For isoprene, the model reproduces both the observed nighttime decline and the subsequent morning growth with a small delay (~1 hour).

The observed declines in isoprene at night (Fig. 6) and above the boundary layer (Fig. 5) reflect its short lifetime against oxidation. We find in the model that OH oxidation accounts for 90% of isoprene loss (Marais et al., 2016), but only 65% of monoterpenes loss (with NO_3 responsible for most of the rest). For isoprene, the subsequent fate of the peroxy radicals ($ISOPO_2$) has been evaluated in detail by Travis et al. (2016), who also present an in-depth analysis of the NO_x budget and impacts on ozone. They show that on average 56% of $ISOPO_2$ reaction during SEAC[4]RS is with NO, and that there is large

spatial variability in this term that is accurately reproduced by the high-resolution GEOS-Chem simulation. Here we focus exclusively on this pathway and the resultant formation of $RONO_2$ from both isoprene and monoterpenes.

3.2 First generation $RONO_2$

Observed near-surface mixing ratios of first generation isoprene nitrates (ISOPN) during SEAC[4]RS are shown in Fig. 7 and are generally well represented by GEOS-Chem ($r = 0.61$; NMB = -0.6%). ISOPN vertical profiles in Fig. 5e indicate a rapid decline from the boundary layer to the free troposphere, reflecting the short atmospheric lifetime (2-4 h in our simulation; Table 1). Comparing the lowest altitude SEAC[4]RS observations to the SOAS median from the CIT-ToF-CIMS (black triangle) indicates an apparent vertical gradient from the surface to ∼500 m. This could be caused by spatial variability between the campaigns, or could reflect rapid dry deposition of ISOPN with limited vertical mixing. GEOS-Chem does not simulate this SOAS-SEAC[4]RS difference, possibly due to overly strong vertical mixing through the modeled boundary layer as identified by Travis et al. (2016) from model comparison to SEACIONS ozonesonde observations.

During SOAS, ISOPN was measured simultaneously by the CIT-ToF-CIMS (Crounse et al., 2006; Nguyen et al., 2015) and the Purdue CIMS (Xiong et al., 2015), and Fig. 6 shows the diurnal cycles from both. Median ISOPN from the Purdue CIMS is a factor of two higher than that from the CIT-ToF-CIMS during daylight hours, with the most significant differences in mid-late morning. In both datasets, ISOPN peaks around 10:00 am local time, is elevated until early evening, and declines to a pre-dawn minimum. Simulated ISOPN from GEOS-Chem is in good agreement with the Purdue CIMS measurements except in the afternoon when modeled ISOPN shows a broad peak (rather than the observed decline) coincident with simulated peak isoprene (Fig. 6). After ∼7:00 pm, the model captures the observed timing of the nighttime ISOPN decline seen in both datasets, as well as the rapid morning growth seen in the Purdue CIMS measurements.

As described in Sect. 2.1, there is considerable uncertainty in the ISOPN yield. We find here that a 9% yield provides the best simulation of the ensemble of SEAC[4]RS and SOAS observations, given experimental constraints on oxidative loss rates (Lee et al., 2014) and dry deposition fluxes (Nguyen et al., 2015). Using model sensitivity studies, we found that applying a lower yield of 7% improved the agreement with the CIT-ToF-CIMS during SOAS, but worsened agreement with the other datasets and is inconsistent with the yields from laboratory experiments (Teng et al., in preparation). We also tested a higher yield of 12%, and found the model overestimated observed SEAC[4]RS and SOAS ISOPN (from both instruments) unless we invoked much larger aerosol uptake and/or added another ISOPN sink. ISOPN sinks (especially aerosol uptake) remain poorly constrained, and the uncertain parameter space describing these processes likely contains multiple solutions that fit the observations equally well (i.e., a higher yield could be accommodated by faster ISOPN loss to aerosol).

Our finding that GEOS-Chem can reproduce the Purdue CIMS ISOPN observations using a 9% ISOPN yield is consistent with the box model of Xiong et al. (2015). The chemical mechanisms used in both studies are similar. In both simulations, modeled ISOPN was overestimated unless an extra sink was included (also consistent with Wolfe et al., 2015, who inferred a missing sink based on SEAC[4]RS flux measurements). While we assumed this sink was due to aerosol uptake, Xiong et al. (2015) invoked enhanced ISOPN photolysis. They argued that models typically underestimate the ISOPN absorption cross section by not taking into account the combined influence of the double bond and hydroxyl group in the ISOPN structure

(Fig. 2). Xiong et al. (2015) were better able to reproduce the observed ISOPN morning peak and afternoon decline when they increased the MCMv3.2 photolysis rate constant by a factor of 5. Including both faster ISOPN photolysis and uptake to the aerosol phase could be a means to accommodate a higher initial ISOPN yield, such as the 12-14% yield inferred from laboratory experiments with the CIT-ToF-CIMS (Teng et al., in preparation), although both sinks remain unverified. The nature
5 of the sink has implications for NO_x recycling from isoprene nitrates (photolysis recycles NO_x while uptake removes it), and this remains a source of uncertainty in our estimates of the impacts of $RONO_2$ on the NO_x budget.

Even more uncertain than ISOPN are the first generation monoterpene nitrates (MONIT). MONIT in GEOS-Chem is a lumped species that represents the sum of monoterpene nitrates from both daytime OH-initiated and nighttime NO_3-initiated oxidation (Sect. 2.2). The nighttime oxidation cascade involves a diversity of reactants (including NO, HO_2, NO_3, and other
10 peroxy radicals) and produces a diversity of monoterpene nitrate species (Lee et al., 2016) that we do not distinguish here. In the model, most MONIT is produced from the NO_3-initiated chemistry, resulting in mean MONIT concentrations of 30-60 ppt at night and $\sim$10-20 ppt during the day.

During SOAS, two monoterpene nitrates were measured by the CIT-ToF-CIMS: $C_{10}H_{17}NO_4$ and $C_{10}H_{17}NO_5$. We find that simulated MONIT shows the same diurnal pattern as the sum of the two measured species (with peak concentrations at
15 night) but is a factor of 2-3 higher (Fig. S3). Pye et al. (2015) similarly found simulated MONIT was a factor of 7 higher than observations using a version of the CMAQ model with explicit MONIT chemistry. The higher modeled values in both studies presumably reflect inclusion in modeled MONIT of many species that were not measured by CIT-ToF-CIMS (including several identified during SOAS by Lee et al., 2016), as well as biases in the model mechanisms (most of the rate constants and products have not been measured). NO_3-initiated monoterpene oxidation is particularly uncertain and is likely too strong
20 in GEOS-Chem, as indicated by large nighttime MONIT overestimates (Fig. S3) combined with monoterpene underestimates (Fig. 6). Simulated nighttime peak values of NO_3-derived isoprene nitrates (ISN1) during SOAS are also up to a factor of 2 higher than the observations reported by Schwantes et al. (2015). This suggests that model biases in nighttime PBL heights and associated vertical mixing may also contribute to simulated nighttime overestimates for some $RONO_2$ species.

3.3 Second generation $RONO_2$ and $pRONO_2$

25 First generation ISOPN and MONIT undergo further oxidation to form a suite of second generation $RONO_2$ species that retain the nitrate functionality (Figs. 2, 3). Four of these species (MVKN, MACRN, PROPNN, and ETHLN) were measured by the CIT-ToF-CIMS, with vertical profiles shown in Fig. 5 (f-h) and spatial distribution shown in Fig. 7. The model provides a good simulation of SEAC⁴RS MVKN+MACRN but underestimates the variability of PROPNN and ETHLN. In contrast, all three species show positive mean model biases relative to the SOAS surface observations. The model tends to overestimate
30 PROPNN and ETHLN at night but underestimate them during the day (Fig. S3), reflecting the assumption in our mechanism that PROPNN is produced at night during NO_3-initiated isoprene oxidation. In reality, the nighttime chemistry produces INs that only photo-oxidize to PROPNN after sunrise (Schwantes et al., 2015). This missing delay between nighttime NO_3 addition and subsequent daytime photo-oxidation likely also explains the model bias relative to the SEAC⁴RS observations, which mostly took place during daytime. Additional simplifications in the NO_3-initiated chemistry could also contribute to

the biases, and preliminary simulations conducted with the AM3 model show that including more details of this chemistry improves model ability to match observed PROPNN (Li et al., in preparation). Some of the bias may also be due to error in the assumed distribution between β- and δ-channel OH-initiated oxidation, as both PROPNN and ETHLN are produced by the latter channel only.

The full time series of first and second generation INs measured at Centreville during SOAS are shown in Fig. 8. We also include the time series of observed particulate $RONO_2$ ($pRONO_2$) estimated from AMS measurements (Fry et al., 2013; Ayres et al., 2015; Lee et al., 2016; Day et al., in preparation) and of ΣANs, the sum of all $RONO_2$ species (including $pRONO_2$) as measured by thermal dissociation laser-induced fluorescence (TD-LIF; Day et al., 2002). Despite the biases identified above, the simulation captures the temporal variability in gas-phase, particulate, and total $RONO_2$ observed over the 6-week campaign, with correlation coefficients of $r \sim 0.6\text{-}0.7$. Low observed and modeled values for all species in early July (days 185-189) indicate suppressed BVOC emissions caused by low temperatures (Marais et al., 2016). The model under-estimates both $pRONO_2$ and ΣANs at night (Fig. S3), suggesting that hydrolysis of particulate monoterpene nitrates should be slower than assumed here (Sect. 2.3). Afternoon overestimates of $pRONO_2$ relative to the AMS observations (Fig. S3) are coincident with the peak in isoprene nitrates (Fig. 6), suggesting overly strong partitioning to the aerosol phase likely due to our assumption of irreversibility (Sect. 2.3).

3.4 $RONO_2$-HCHO relationship

The relationship between organic nitrates and formaldehyde (HCHO), a high-yield product of the $ISOPO_2$ + NO reaction, provides an additional test of the model chemistry and in particular the IN yield. Daytime isoprene oxidation in the presence of NO_x co-produces HCHO and INs, resulting in an expected strong correlation between these species (Perring et al., 2009a). When INs dominate total $RONO_2$, the correlation should also be strong between HCHO and ΣANs, and this relationship has previously been used to constrain the IN yield when IN measurements were not available. For example, HCHO and ΣANs measurements from the 2004 ICARTT aircraft campaign showed moderate correlation with $r \sim 0.4\text{-}0.6$ (Perring et al., 2009a; Mao et al., 2013). However, linking the HCHO-ΣANs correlation to the IN yield is complicated by the contribution to ΣANs from other $RONO_2$ sources (e.g., monoterpene nitrates, anthropogenic nitrates, etc.). During SEAC[4]RS, a better constraint can be obtained directly from the HCHO-IN relationship. Figure 9 shows the correlation between HCHO and the sum of ISOPN, MVKN, and MACRN (we exclude PROPNN and ETHLN to avoid the biases identified previously). The figure shows the observed slope of 0.027 (ppt IN) (ppt HCHO)$^{-1}$ is reproduced by the model but with more scatter in the simulation ($r \sim 0.5$) than in the observations ($r \sim 0.7$). The similarity of the observed and simulated relationships in Fig. 9 lends confidence to the IN mechanism used here, at least for the β-peroxy channel.

4 Total alkyl and multifunctional nitrates (ΣANs)

4.1 Speciated versus total $RONO_2$

SEAC^{4}RS represents one of the first airborne campaigns to make measurements of individual BVOC-derived $RONO_2$ species. Without these speciated measurements, previous model evaluations of isoprene nitrate chemistry have relied on TD-LIF obser-
vations of ΣANs (total $RONO_2$), with the assumption that gas-phase INs account for the majority of ΣANs (Horowitz et al., 2007; Perring et al., 2009a; Mao et al., 2013; Xie et al., 2013). Figure 10a compares the TD-LIF ΣANs measurement (solid line) to the sum of explicitly measured gas-phase $RONO_2$ species and total $pRONO_2$ (dashed line, combined CIT-ToF-CIMS, WAS, and AMS measurements) during SEAC^{4}RS. The figure shows a large gap between measured ΣANs and the total of speciated $RONO_2$ (including both gas-phase and aerosol contributions), especially near the surface (ΣANs = 409 ppt, total speciated $RONO_2$ = 198 ppt). Figure 10a also shows the median surface ΣANs measured during SOAS (198 ppt; black trian-
gle). As for SEAC^{4}RS, SOAS total speciated $RONO_2$ is much lower (82 ppt) when calculated from the CIT-ToF-CIMS and AMS measurements. The gap is smaller, but still exists, when calculated using ISOPN from the Purdue CIMS (total $RONO_2$ = 102 ppt) or $pRONO_2$ from the TD-LIF (total $RONO_2$ = 139 ppt). An independent thermal dissociation instrument operated by the SouthEastern Aerosol Research and Characterization (SEARCH) Network also measured ΣANs at the SOAS site and showed values that were 80 ppt higher than measured by the TD-LIF (but generally well correlated, with slope close to 1 and $r \sim 0.8$).

Some of the difference between the total speciated $RONO_2$ and ΣANs measurements can be attributed to gas-phase nitrates not measured by CIT-ToF-CIMS or WAS. A number of these were identified during SOAS using a second ToF-CIMS operated by the University of Washington (Lee et al., 2016). In addition, SEAC^{4}RS observations of total NO_y ($\equiv NO_x + HNO_3 + PAN + RONO_2$, including $pRONO_2$) are better balanced by including the ΣANs than the speciated $RONO_2$ components ($\approx$81% vs. 70% of surface NO_y, compared to 56% with no $RONO_2$ contribution). Also contributing to the discrepancy are the large uncertainties still associated with $RONO_2$ measurement techniques. Lee et al. (2016) found that SOAS measurements of $pRONO_2$ differ by factors of 2-4, as also shown in Fig. S3, with the AMS lower than TD-LIF. Similarly, we showed in Sect. 3 that the two SOAS measurements of ISOPN differ by up to a factor of 2 (CIT-ToF-CIMS lower than Purdue CIMS, for reasons that remain unclear). Assuming similar uncertainties characterize the SEAC^{4}RS $RONO_2$ measurements, these could readily explain some of the inability of the speciated measurements to close the ΣANs budget in Fig. 10a.

Comparison of GEOS-Chem to the two total $RONO_2$ estimates in Fig. 10a shows that the model greatly underestimates SEAC^{4}RS ΣANs relative to the TD-LIF measurement, with a much smaller underestimate relative to the speciated sum. The better fit to the speciated measurements than to the ΣANs is consistent with the model's ability to match both individual gas-phase $RONO_2$ species measured by the CIT-ToF-CIMS and total $pRONO_2$ measured by the AMS (Sect. 3). During SOAS, Fig. 8 shows that GEOS-Chem can reproduce much of the temporal variability in the ΣANs ($r = 0.57$) with little bias.

4.2 RONO₂ composition

Figure 10b compares the observed and simulated $RONO_2$ composition in the Southeast US during SEAC[4]RS. For clarity, only the speciated measurements are shown in the figure. The observations show a constant 20-30 ppt background at all altitudes from small (C_1-C_3) $RONO_2$ produced from anthropogenic VOCs. The contributions of these small nitrates are consistent with the observed concentrations of their parent VOCs and with known reaction rate constants (Atkinson and Arey, 2003), $RONO_2$ yields (Perring et al., 2013), and $RONO_2$ lifetimes (Talukdar et al., 1997; Dahl et al., 2005; Worton et al., 2010) assuming steady state. GEOS-Chem does not simulate these nitrates under the assumption that their contributions to total NO_y are insignificant. The SEAC[4]RS data clearly show that this assumption is not valid, at least for the US where natural gas production is a large alkane source, and is contributing to model bias in both $RONO_2$ and NO_y. Given the long lifetimes (weeks-months) of the small nitrates, the bias is particularly acute in the free troposphere and has implications for global N export.

In both observations and model, gas-phase INs (orange) account for half of speciated $RONO_2$ (25% of ΣANs), split roughly equally between 1st and 2nd generation species. The model underestimates somewhat the 2nd generation INs, as seen previously in Figs. 5 and 7. In the model, gas-phase MTNs from monoterpenes (blue; not measured during SEAC[4]RS) account for an additional 10% of simulated $RONO_2$ ($\sim$5% relative to ΣANs). Previous studies during ICARTT also found a 10% MTN contribution to $RONO_2$ (Horowitz et al., 2007; Perring et al., 2009a), although MTNs have been neglected in more recent simulations (e.g., Mao et al., 2013; Xie et al., 2013). Other C_4-C_5 nitrates (yellow, including alkyl nitrates from WAS and alkene hydroxynitrates from CIT-ToF-CIMS) similarly contribute 5-10% of observed $RONO_2$; these are underestimated by 50% in GEOS-Chem because the model does not include nitrate formation from anthropogenic alkenes.

A significant fraction (10-20%) of $RONO_2$ was in the aerosol phase during SEAC[4]RS. The model underestimates the observed $pRONO_2$ contribution in the free troposphere; however, some caution should be used when interpreting these data. Observed $pRONO_2$ is the product of measured total aerosol nitrate and the measured organic fraction of the nitrate aerosol, but during SEAC[4]RS the organic fraction was often not reported in the free troposphere due to interference from dust layers and instrumental issues. In these instances, the organic fraction of measured nitrate is assumed to be 0.8, based largely on surface measurements from multiple campaigns (Day et al., in preparation). In the free troposphere (>1.5 km), this assumption is applied to 85% of the SEAC[4]RS 1-minute data, and could lead to a high bias in the $pRONO_2$ observations. Nonetheless, it is also likely that simulated $pRONO_2$ is underestimated because of our assumption that all $pRONO_2$ species undergo rapid hydrolysis. In fact, many of the nitrates produced from BVOC oxidation are not expected to hydrolyze at all (Boyd et al., 2015; Pye et al., 2015) and so would have lifetimes sufficiently long for export out of the boundary layer.

Our simulated $RONO_2$ composition in Fig. 10b suggests a less important role for INs than identified from recent simulations of the ICARTT data. In an earlier version of GEOS-Chem, INs alone could explain all measured ΣANs during ICARTT ($\sim$200 ppt at the surface; Mao et al., 2013), and both that model and a CMAQ simulation (Xie et al., 2013) suggested INs were dominated by 2nd generation species (70-90% of total INs). These earlier simulations did not account for either aerosol uptake and possible hydrolysis (Darer et al., 2011; Jacobs et al., 2014) or fast photolysis (Müller et al., 2014) of 2nd generation

INs, and so lifetimes were significantly longer than in our simulation. We performed sensitivity simulations without these additional IN sinks and found that the model overestimated observed 2nd generation INs by a factor of 3-5 during SEAC[4]RS. It seems likely that 2nd generation IN overestimates in previous work were compensated for by omitting the contributions from MTNs and $pRONO_2$. Here, we find MTN and $pRONO_2$ combined contribute as much to total $RONO_2$ as either 1st or

5   2nd generation INs alone, and that excluding them would lead to major model shortcomings. The $pRONO_2$ contribution is especially important as different removal processes for gas-phase versus particulate species would have different implications for NO_x budgets and N deposition.

5   Fate of organic nitrates and implications for nitrogen budgets

Table 1 summarizes the dominant fates and lifetimes of individual gas-phase $RONO_2$ in the Southeast US boundary layer

10   during the SEAC[4]RS campaign (12 Aug - 23 Sep) as calculated from GEOS-Chem. The contribution of different fates to total gas-phase $RONO_2$ loss is illustrated in Fig. 11a. Loss processes that recycle $RONO_2$ by converting between $RONO_2$ species (e.g., from first to second generation) are not included. Total simulated $RONO_2$ loss is dominated by aerosol hydrolysis, with an additional large loss to deposition that is consistent with the rapid deposition fluxes of both INs and MTNs observed during SOAS (Nguyen et al., 2015). The large predicted losses to aerosol influence simulation of both $pRONO_2$ (for which uptake is

15   the only source in the model) and HNO_3 (which is produced during $pRONO_2$ hydrolysis). We find here that our simulation including a large sink to aerosol is consistent with observed surface $pRONO_2$ concentrations and variability (Figs. 8 and 10), HNO_3 concentrations (Travis et al., 2016, Fig. 2), and nitrate wet deposition fluxes (Travis et al., 2016, Fig. 3) during SEAC[4]RS and SOAS.

Overall, more than 80% of simulated gas-phase $RONO_2$ are lost via processes that irreversibly remove nitrogen from the

20   atmosphere (deposition, aerosol hydrolysis). The remainder is primarily lost via photolysis, driven largely by the fast photolysis of 2nd generation carbonyl INs (Müller et al., 2014). Romer et al. (2016) similarly found that terminal NO_x sinks dominated $RONO_2$ loss processes during SOAS, responsible for 55% $\pm$ 20% of total loss, primarily due to aerosol hydrolysis. $RONO_2$ lifetimes are too short (minutes-hours, Table 1 and Romer et al., 2016) for significant transport to occur, and simulated $RONO_2$ loss typically occurs only a short distance from sources. Summed over the Southeast US domain, we find gross $RONO_2$

25   production and loss are roughly balanced (640 Mg N d^{-1}). This balance implies that BVOC-derived gas-phase $RONO_2$ are not generally exported from the Southeast US, in agreement with earlier work (Horowitz et al., 2007; Hudman et al., 2007; Fang et al., 2010; Mao et al., 2013). However, this calculation excludes the longer-lived small alkyl nitrates and non-hydrolyzing particulate nitrates not simulated in GEOS-Chem (Sect. 4). These may be an important source of exported reactive nitrogen, and their inclusion should be a priority for future model development.

30   The impacts of $RONO_2$ production and other loss processes on the NO_x budget are shown in Fig. 11b for the Southeast US boundary layer in August-September 2013. Non-$RONO_2$ losses in the figure are mainly HNO_3 formation, with an additional contribution from PANs (relevant in regions with elevated NO_x; Browne and Cohen, 2012). We find in the model that gross NO_x loss due to $RONO_2$ production is 35 Gg N over this period. As shown in Fig. 11a, only 23% of this $RONO_2$ (8 Gg N)

goes on to recycle NO_x. We therefore find that $RONO_2$ production serves as a net NO_x sink of 27 Gg N in the Southeast US in summer, equivalent to 21% of NO_x emitted in this region and season.

These regional-scale averages conceal important spatial variability. Figure 12 shows how the NO_x sink due to $RONO_2$ production varies spatially across the Southeast US in summer, and how this depends on the ratio between BVOC and NO_x emissions (E_{BVOC}/E_{NOx}). The fractional NO_x sink to $RONO_2$ is strongly correlated ($r = 0.90$) to the E_{BVOC}/E_{NOx} ratio. Our finding that $RONO_2$ production dominates NO_x loss in very low NO_x environments is consistent with an earlier analysis for boreal Canada (Browne and Cohen, 2012), which found the fractional sink to $RONO_2$ approached unity for $[NO_x] < 50$ ppt, and with analysis of a subset of the SEAC[4]RS data from the low-NO_x Ozarks Mountains (Wolfe et al., 2015).

Figure 12c shows how the fractional NO_x sink to $RONO_2$ (blue) and the E_{BVOC}/E_{NOx} emission ratio (red) vary as a function of NO_x emissions (gray, shown as their cumulative distribution binned into 5% quantiles). Both are inversely related to NO_x emissions. We see from the figure that $RONO_2$ production is the dominant NO_x sink for regions that account for the lowest 5% of total Southeast US NO_x emissions (leftmost bar in Fig. 12c), but the importance of the sink drops off rapidly as NO_x emissions increase. By the time 30% of the regional NO_x emissions are accounted for, the fractional sink has dropped to 0.2, and from there continues to decline to a minimum of 0.03 in the highest-emitting regions.

The mean E_{BVOC}/E_{NOx} ratio averaged over the Southeast US is 5.3 and is highlighted as the white point in Fig. 12c. The figure shows that most Southeast US NO_x emission (~65%) occurs at E_{BVOC}/E_{NOx} ratios that are significantly lower than the regional mean, highlighting the significant spatial segregation between NO_x and BVOC emissions in this region (Yu et al., 2016).

Emissions projections for the Southeast US anticipate continued decreases in NO_x emissions (and concomitant increases in the E_{BVOC}/E_{NOx} ratio). While these changes should increase the importance of $RONO_2$ for the NO_x budget, the relationship shown in Fig. 12c suggests very large emissions decreases will be necessary before $RONO_2$ becomes a major regional sink for NOx. The figure shows that the sink to $RONO_2$ is only sensitive to NO_x emissions in regions where they are already low: a 10% decrease in total Southeast US NO_x emissions (e.g., a leftward shift by two bars in the figure) would increase the importance of the sink by less than 0.5%. The actual rate at which NO_x emissions in the Southeast US will decrease varies widely among different projections. Under the Representative Concentration Pathway 8.5 (RCP8.5), for example, the Southeast US would see a decrease (relative to 2013 emissions) of 45% by 2050 to ~1300 Mg N d^{-1}; according to Fig. 12, the $RONO_2$ sink would still only account for about 10% of the loss in the highest emitting regions. Under the more aggressive RCP4.5, emissions would decline by 65% to ~800 Mg N day^{-1} in 2050. At this stage, the $RONO_2$ sink would become significant (>20%) throughout the region.

6 Conclusions

We have used airborne and ground-based observations from two summer 2013 campaigns in the Southeast US (SEAC[4]RS, SOAS) to better understand the chemistry and impacts of alkyl and multi-functional organic nitrates ($RONO_2$). We used the observations, along with findings from recent laboratory, field, and modeling studies, to update and evaluate biogenic

volatile organic compound (BVOC) oxidation schemes in the GEOS-Chem chemical transport model (CTM). From there, we used the updated CTM with $0.25° \times 0.3125°$ ($\sim 25 \times 25$ km^2) horizontal resolution to examine $RONO_2$ speciation, chemical production/loss processes, and importance as a sink for NO_x.

Our improved mechanism provides a state-of-the-science description of isoprene oxidation in the presence of NO_x, with updates including a 9% isoprene nitrate (IN) yield (Xiong et al., 2015), an increase in the population of β- vs δ-hydroxyl isomers (Peeters et al., 2014), revised IN reaction rate constants and products (Jacobs et al., 2014; Lee et al., 2014), fast photolysis of carbonyl INs (Müller et al., 2014), rapid IN dry deposition (Nguyen et al., 2015), and a simplified scheme for aerosol partitioning of soluble INs (Xu et al., 2014; Marais et al., 2016) followed by particle-phase hydrolysis (Jacobs et al., 2014; Rindelaub et al., 2015). For the first time in GEOS-Chem, we have also added both OH- and NO_3-initiated monoterpene oxidation leading to the formation of monoterpene nitrates (MTNs), with similar loss processes as for INs. With these updates, GEOS-Chem simulates surface-level BVOC and $RONO_2$ mixing ratios that are generally within the observed variability of the SEAC^{4}RS and SOAS data.

Observed first generation IN (ISOPN) variability is generally reproduced without bias by GEOS-Chem, except at midday when modeled ISOPN peaks while SOAS observations indicate a gradual decline. For second generation INs, the model shows more skill for species produced primarily from β–hydroxyl isomers (MVKN+MACRN) than those from δ-hydroxyl isomers and NO_3-initiated chemistry (PROPNN+ETHLN). For the latter, GEOS-Chem underestimates both magnitudes and variability relative to the SEAC^{4}RS observations. While this could imply a more important role for δ-channel oxidation than included in our mechanism, theoretical considerations suggest that our assumed δ-hydroxyl contribution is already an upper limit (Peeters et al., 2014), and more measurements are needed to reconcile these theoretical and observational constraints. Better understanding of nighttime NO_3-initiated isoprene oxidation could also play an important role in improving simulation of second generation INs.

The SEAC^{4}RS observations imply that gas-phase INs account for 25-50% of total surface $RONO_2$, much less than inferred from previous modeling studies (Mao et al., 2013; Xie et al., 2013). GEOS-Chem reproduces this contribution and attributes an additional 10% of $RONO_2$ to MTNs. Both observations and model show 10-20% of the remaining $RONO_2$ at the surface is in the particle phase (p$RONO_2$). In the free troposphere, GEOS-Chem greatly underestimates total $RONO_2$ by ignoring contributions from small, long-lived nitrates derived from anthropogenic VOCs and from non-hydrolyzing particulate species. This has a significant impact on simulation of reactive nitrogen export from the United States and should be remedied in future model development.

We find in the model that formation of p$RONO_2$ via aerosol uptake, followed by particle-phase hydrolysis, is the dominant loss process for gas-phase $RONO_2$. Including this large sink to aerosol results in simulated $RONO_2$, p$RONO_2$ and HNO_3 mixing ratios and nitrate deposition fluxes that are consistent with observations. $RONO_2$ loss via deposition is also significant, with $RONO_2$ (both gas-phase and particulate) responsible for $\sim$3% of total N deposition over the Southeast US in summer.

Overall, less than a quarter of simulated gas-phase $RONO_2$ loss recycles atmospheric NO_x. We find in the model that $RONO_2$ production accounts for 21% of the net sink of NO_x emitted in the Southeast US in summer. $RONO_2$ production is the dominant NO_x sink only in regions where elevated BVOC emissions are paired with very low NO_x emissions. Elsewhere,

the importance of the sink declines rapidly as a function of NO_x emissions. Most of the Southeast US NO_x is emitted in locations where BVOC emissions are relatively low, limiting the importance of $RONO_2$ as a NO_x sink.

Southeast US NO_x emissions have been declining for the past two decades (Hidy et al., 2014; Simon et al., 2015) and further reductions are projected (Lamarque et al., 2011; EPA, 2014). Previous studies have suggested these declines will trigger a more

5 important role for $RONO_2$ as a NO_x sink in future (Browne and Cohen, 2012). In contrast, we find here that the NO_x sink to $RONO_2$ is only sensitive to NO_x emissions in regions where they are already low because of the spatial segregation between NO_x and BVOC emissions. We find that a 10% decrease in Southeast US NO_x emissions would enhance the importance of this sink by less than 0.5%. HNO_3 formation and deposition is likely to remain the dominant sink for NO_x even as NO_x emissions decrease.

10 *Acknowledgements.* We are grateful to the entire NASA SEAC[4]RS team for their help in the field, and we thank Eleanor Browne and Fabien Paulot for helpful discussions about the monoterpene nitrate scheme. This work was funded by a University of Wollongong Vice Chancellor's Postdoctoral Fellowship to JAF and by the NASA Tropospheric Chemistry Program. This research was undertaken with the assistance of resources provided at the NCI National Facility systems at the Australian National University through the National Computational Merit Allocation Scheme supported by the Australian Government. JM acknowledge supports from the NOAA Climate Program Office grant

15 NA13OAR4310071. JLJ, PCJ, WH, and DAD were supported by NASA NNX15AH33A and NNX15AT96G, NSF AGS-1243354 and AGS-1360834, and EPRI 10004734. Isoprene and monoterpene measurements during SEAC[4]RS were supported by the Austrian Federal Ministry for Transport, Innovation and Technology (bmvit) through the Austrian Space Applications Programme (ASAP) of the Austrian Research Promotion Agency (FFG). AW and TM received support from the Visiting Scientist Program at the National Institute of Aerospace (NIA).

References

Amos, H. M., Jacob, D. J., Holmes, C. D., Fisher, J. A., Wang, Q., Yantosca, R. M., Corbitt, E. S., Galarneau, E., Rutter, A. P., Gustin, M. S., Steffen, A., Schauer, J. J., Graydon, J. A., Louis, V. L. S., Talbot, R. W., Edgerton, E. S., Zhang, Y., and Sunderland, E. M.: Gas-particle partitioning of atmospheric Hg(II) and its effect on global mercury deposition, Atmospheric Chemistry and Physics, 12, 591–603, doi:10.5194/acp-12-591-2012, http://www.atmos-chem-phys.net/12/591/2012/, 2012.

Aschmann, S. M., Atkinson, R., and Arey, J.: Products of reaction of OH radicals with $alpha$-pinene, J. Geophys. Res., 107, doi:10.1029/2001jd001098, http://dx.doi.org/10.1029/2001JD001098, 2002.

Atkinson, R. and Arey, J.: Atmospheric Degradation of Volatile Organic Compounds, Chemical Reviews, 103, 4605–4638, doi:10.1021/cr0206420, http://dx.doi.org/10.1021/cr0206420, pMID: 14664626, 2003.

Ayres, B. R., Allen, H. M., Draper, D. C., Brown, S. S., Wild, R. J., Jimenez, J. L., Day, D. A., Campuzano-Jost, P., Hu, W., de Gouw, J., Koss, A., Cohen, R. C., Duffey, K. C., Romer, P., Baumann, K., Edgerton, E., Takahama, S., Thornton, J. A., Lee, B. H., Lopez-Hilfiker, F. D., Mohr, C., Wennberg, P. O., Nguyen, T. B., Teng, A., Goldstein, A. H., Olson, K., and Fry, J. L.: Organic nitrate aerosol formation via NO_3 + biogenic volatile organic compounds in the southeastern United States, Atmospheric Chemistry and Physics, 15, 13 377–13 392, doi:10.5194/acp-15-13377-2015, http://www.atmos-chem-phys.net/15/13377/2015/, 2015.

Barnes, I., Becker, K. H., and Zhu, T.: Near UV absorption spectra and photolysis products of difunctional organic nitrates: Possible importance as NO x reservoirs, Journal of Atmospheric Chemistry, 17, 353–373, doi:10.1007/BF00696854, http://dx.doi.org/10.1007/BF00696854, 1993.

Beaver, M. R., St. Clair, J. M., Paulot, F., Spencer, K. M., Crounse, J. D., LaFranchi, B. W., Min, K. E., Pusede, S. E., Wooldridge, P. J., Schade, G. W., Park, C., Cohen, R. C., and Wennberg, P. O.: Importance of biogenic precursors to the budget of organic nitrates: observations of multifunctional organic nitrates by CIMS and TD-LIF during BEARPEX 2009, Atmospheric Chemistry and Physics, 12, 5773–5785, doi:10.5194/acp-12-5773-2012, http://www.atmos-chem-phys.net/12/5773/2012/, 2012.

Boyd, C. M., Sanchez, J., Xu, L., Eugene, A. J., Nah, T., Tuet, W. Y., Guzman, M. I., and Ng, N. L.: Secondary organic aerosol formation from the β-pinene+NO_3 system: effect of humidity and peroxy radical fate, Atmospheric Chemistry and Physics, 15, 7497–7522, doi:10.5194/acp-15-7497-2015, http://www.atmos-chem-phys.net/15/7497/2015/, 2015.

Brown, S. S., deGouw, J. A., Warneke, C., Ryerson, T. B., Dubé, W. P., Atlas, E., Weber, R. J., Peltier, R. E., Neuman, J. A., Roberts, J. M., Swanson, A., Flocke, F., McKeen, S. A., Brioude, J., Sommariva, R., Trainer, M., Fehsenfeld, F. C., and Ravishankara, A. R.: Nocturnal isoprene oxidation over the Northeast United States in summer and its impact on reactive nitrogen partitioning and secondary organic aerosol, Atmospheric Chemistry and Physics, 9, 3027–3042, doi:10.5194/acp-9-3027-2009, http://www.atmos-chem-phys.net/9/3027/2009/, 2009.

Brown, S. S., Dubé, W. P., Bahreini, R., Middlebrook, A. M., Brock, C. A., Warneke, C., de Gouw, J. A., Washenfelder, R. A., Atlas, E., Peischl, J., Ryerson, T. B., Holloway, J. S., Schwarz, J. P., Spackman, R., Trainer, M., Parrish, D. D., Fehshenfeld, F. C., and Ravishankara, A. R.: Biogenic VOC oxidation and organic aerosol formation in an urban nocturnal boundary layer: aircraft vertical profiles in Houston, TX, Atmospheric Chemistry and Physics, 13, 11 317–11 337, doi:10.5194/acp-13-11317-2013, http://www.atmos-chem-phys.net/13/11317/2013/, 2013.

Browne, E. C. and Cohen, R. C.: Effects of biogenic nitrate chemistry on the NO_x lifetime in remote continental regions, Atmospheric Chemistry and Physics, 12, 11 917–11 932, doi:10.5194/acp-12-11917-2012, http://dx.doi.org/10.5194/acp-12-11917-2012, 2012.

Browne, E. C., Wooldridge, P. J., Min, K.-E., and Cohen, R. C.: On the role of monoterpene chemistry in the remote continental boundary layer, Atmospheric Chemistry and Physics, 14, 1225–1238, doi:10.5194/acp-14-1225-2014, http://dx.doi.org/10.5194/acp-14-1225-2014, 2014.

Chen, X., Hulbert, D., and Shepson, P. B.: Measurement of the organic nitrate yield from OH reaction with isoprene, Journal of Geophysical Research: Atmospheres (1984–2012), 103, 25 563–25 568, 1998.

Crounse, J. D., McKinney, K. A., Kwan, A. J., and Wennberg, P. O.: Measurement of Gas-Phase Hydroperoxides by Chemical Ionization Mass Spectrometry, Analytical Chemistry, 78, 6726–6732, doi:10.1021/ac0604235, http://dx.doi.org/10.1021/ac0604235, pMID: 17007490, 2006.

Dahl, E. E., Yvon-Lewis, S. A., and Saltzman, E. S.: Saturation anomalies of alkyl nitrates in the tropical Pacific Ocean, Geophysical Research Letters, 32, n/a–n/a, doi:10.1029/2005GL023896, http://dx.doi.org/10.1029/2005GL023896, l20817, 2005.

Darer, A. I., Cole-Filipiak, N. C., O'Connor, A. E., and Elrod, M. J.: Formation and Stability of Atmospherically Relevant Isoprene-Derived Organosulfates and Organonitrates, Environmental Science & Technology, 45, 1895–1902, doi:10.1021/es103797z, http://dx.doi.org/10.1021/es103797z, pMID: 21291229, 2011.

Day, D. A., Wooldridge, P. J., Dillon, M. B., Thornton, J. A., and Cohen, R. C.: A thermal dissociation laser-induced fluorescence instrument for in situ detection of NO2, peroxy nitrates, alkyl nitrates, and HNO3, Journal of Geophysical Research: Atmospheres, 107, ACH 4–1–ACH 4–14, doi:10.1029/2001JD000779, http://dx.doi.org/10.1029/2001JD000779, 2002.

Day, D. A., Liu, S., Russell, L. M., and Ziemann, P. J.: Organonitrate group concentrations in submicron particles with high nitrate and organic fractions in coastal southern California, Atmospheric Environment, 44, 1970 – 1979, doi:http://dx.doi.org/10.1016/j.atmosenv.2010.02.045, http://www.sciencedirect.com/science/article/pii/S1352231010001846, 2010.

Day, D. A., Campuzano-Jost, P., Palm, B. B., Hu, W., Nault, B. A., Wooldridge, P. J., Cohen, R. C., Docherty, K. S., Wagner, N. L., and Jimenez, J.-L.: Observations of particle organic nitrate from airborne and ground platforms in North America: Insights into vertical and geographical distributions, gas/particle partitioning, losses, and contributions to total particle nitrate, in preparation.

EPA: U.S. Environmental Protection Agency, Technical Support Document (TSD): preparation of Emissions Inventories for the Version 6.1, 2011 Emissions Modeling Platform, Tech. rep., U.S. Environmental Protection Agency, 2014.

Fang, Y., Fiore, A. M., Horowitz, L. W., Levy, H., Hu, Y., and Russell, A. G.: Sensitivity of the NOy budget over the United States to anthropogenic and lightning NOx in summer, Journal of Geophysical Research: Atmospheres, 115, n/a–n/a, doi:10.1029/2010JD014079, http://dx.doi.org/10.1029/2010JD014079, d18312, 2010.

Fiore, A. M., Horowitz, L. W., Purves, D. W., Levy, H., Evans, M. J., Wang, Y., Li, Q., and Yantosca, R. M.: Evaluating the contribution of changes in isoprene emissions to surface ozone trends over the eastern United States, Journal of Geophysical Research: Atmospheres, 110, n/a–n/a, doi:10.1029/2004JD005485, http://dx.doi.org/10.1029/2004JD005485, d12303, 2005.

Fischer, E. V., Jacob, D. J., Yantosca, R. M., Sulprizio, M. P., Millet, D. B., Mao, J., Paulot, F., Singh, H. B., Roiger, A., Ries, L., Talbot, R., Dzepina, K., and Pandey Deolal, S.: Atmospheric peroxyacetyl nitrate (PAN): a global budget and source attribution, Atmospheric Chemistry and Physics, 14, 2679–2698, doi:10.5194/acp-14-2679-2014, http://www.atmos-chem-phys.net/14/2679/2014/, 2014.

Fry, J. L., Kiendler-Scharr, A., Rollins, A. W., Wooldridge, P. J., Brown, S. S., Fuchs, H., Dubé, W., Mensah, A., dal Maso, M., Tillmann, R., Dorn, H.-P., Brauers, T., and Cohen, R. C.: Organic nitrate and secondary organic aerosol yield from NO$_3$ oxidation of Î²-pinene evaluated using a gas-phase kinetics/aerosol partitioning model, Atmospheric Chemistry and Physics, 9, 1431–1449, doi:10.5194/acp-9-1431-2009, http://www.atmos-chem-phys.net/9/1431/2009/, 2009.

Fry, J. L., Draper, D. C., Zarzana, K. J., Campuzano-Jost, P., Day, D. A., Jimenez, J. L., Brown, S. S., Cohen, R. C., Kaser, L., Hansel, A., Cappellin, L., Karl, T., Hodzic Roux, A., Turnipseed, A., Cantrell, C., Lefer, B. L., and Grossberg, N.: Observations of gas- and aerosol-phase organic nitrates at BEACHON-RoMBAS 2011, Atmospheric Chemistry and Physics, 13, 8585–8605, doi:10.5194/acp-13-8585-2013, http://www.atmos-chem-phys.net/13/8585/2013/, 2013.

5 Fry, J. L., Draper, D. C., Barsanti, K. C., Smith, J. N., Ortega, J., Winkler, P. M., Lawler, M. J., Brown, S. S., Edwards, P. M., Cohen, R. C., and Lee, L.: Secondary Organic Aerosol Formation and Organic Nitrate Yield from NO 3 Oxidation of Biogenic Hydrocarbons, Environmental Science & Technology, 48, 11 944–11 953, doi:10.1021/es502204x, http://dx.doi.org/10.1021/es502204x, 2014.

Goliff, W. S., Stockwell, W. R., and Lawson, C. V.: The regional atmospheric chemistry mechanism, version 2, Atmospheric Environment, 68, 174 – 185, doi:http://dx.doi.org/10.1016/j.atmosenv.2012.11.038, http://www.sciencedirect.com/science/article/pii/S1352231012011065,

10 2013.

Guenther, A. B., Jiang, X., Heald, C. L., Sakulyanontvittaya, T., Duhl, T., Emmons, L. K., and Wang, X.: The Model of Emissions of Gases and Aerosols from Nature version 2.1 (MEGAN2.1): an extended and updated framework for modeling biogenic emissions, Geoscientific Model Development, 5, 1471–1492, doi:10.5194/gmd-5-1471-2012, http://www.geosci-model-dev.net/5/1471/2012/, 2012.

Hidy, G. M., Blanchard, C. L., Baumann, K., Edgerton, E., Tanenbaum, S., Shaw, S., Knipping, E., Tombach, I., Jansen, J., and Wal-

15 ters, J.: Chemical climatology of the southeastern United States, 1999-2013, Atmospheric Chemistry and Physics, 14, 11 893–11 914, doi:10.5194/acp-14-11893-2014, http://dx.doi.org/10.5194/acp-14-11893-2014, 2014.

Horowitz, L. W., Liang, J., Gardner, G. M., and Jacob, D. J.: Export of reactive nitrogen from North America during summertime: Sensitivity to hydrocarbon chemistry, Journal of Geophysical Research: Atmospheres (1984–2012), 103, 13 451–13 476, 1998.

Horowitz, L. W., Fiore, A. M., Milly, G. P., Cohen, R. C., Perring, A., Wooldridge, P. J., Hess, P. G., Emmons, L. K., and Lamar-

20 que, J.-F.: Observational constraints on the chemistry of isoprene nitrates over the eastern United States, J. Geophys. Res., 112, doi:10.1029/2006jd007747, http://dx.doi.org/10.1029/2006JD007747, 2007.

Hu, K. S., Darer, A. I., and Elrod, M. J.: Thermodynamics and kinetics of the hydrolysis of atmospherically relevant organonitrates and organosulfates, Atmospheric Chemistry and Physics, 11, 8307–8320, doi:10.5194/acp-11-8307-2011, http://www.atmos-chem-phys.net/11/8307/2011/, 2011.

25 Hudman, R. C., Jacob, D. J., Turquety, S., Leibensperger, E. M., Murray, L. T., Wu, S., Gilliland, A. B., Avery, M., Bertram, T. H., Brune, W., Cohen, R. C., Dibb, J. E., Flocke, F. M., Fried, A., Holloway, J., Neuman, J. A., Orville, R., Perring, A., Ren, X., Sachse, G. W., Singh, H. B., Swanson, A., and Wooldridge, P. J.: Surface and lightning sources of nitrogen oxides over the United States: Magnitudes, chemical evolution, and outflow, Journal of Geophysical Research: Atmospheres, 112, n/a–n/a, doi:10.1029/2006JD007912, http://dx.doi.org/10.1029/2006JD007912, d12S05, 2007.

30 Jacobs, M. I., Burke, W. J., and Elrod, M. J.: Kinetics of the reactions of isoprene-derived hydroxynitrates: gas phase epoxide formation and solution phase hydrolysis, Atmospheric Chemistry and Physics, 14, 8933–8946, doi:10.5194/acp-14-8933-2014, http://www.atmos-chem-phys.net/14/8933/2014/, 2014.

Kim, H., Barkey, B., and Paulson, S. E.: Real Refractive Indices and Formation Yields of Secondary Organic Aerosol Generated from Photooxidation of Limonene and α-Pinene: The Effect of the HC/NO x Ratio, J. Phys. Chem. A, 116, 6059–6067, doi:10.1021/jp301302z,

35 http://dx.doi.org/10.1021/jp301302z, 2012.

Kim, P. S., Jacob, D. J., Fisher, J. A., Travis, K., Yu, K., Zhu, L., Yantosca, R. M., Sulprizio, M. P., Jimenez, J. L., Campuzano-Jost, P., Froyd, K. D., Liao, J., Hair, J. W., Fenn, M. A., Butler, C. F., Wagner, N. L., Gordon, T. D., Welti, A., Wennberg, P. O., Crounse, J. D., St. Clair, J. M., Teng, A. P., Millet, D. B., Schwarz, J. P., Markovic, M. Z., and Perring, A. E.: Sources, seasonality, and trends of southeast US

aerosol: an integrated analysis of surface, aircraft, and satellite observations with the GEOS-Chem chemical transport model, Atmospheric Chemistry and Physics, 15, 10 411–10 433, doi:10.5194/acp-15-10411-2015, http://www.atmos-chem-phys.net/15/10411/2015/, 2015.

Knote, C., Hodzic, A., and Jimenez, J. L.: The effect of dry and wet deposition of condensable vapors on secondary organic aerosols concentrations over the continental US, Atmospheric Chemistry and Physics, 15, 1–18, doi:10.5194/acp-15-1-2015, http://www.atmos-chem-phys.net/15/1/2015/, 2015.

Lamarque, J.-F., Kyle, G., Meinshausen, M., Riahi, K., Smith, S., van Vuuren, D., Conley, A., and Vitt, F.: Global and regional evolution of short-lived radiatively-active gases and aerosols in the Representative Concentration Pathways, Climatic Change, 109, 191–212, doi:10.1007/s10584-011-0155-0, http://dx.doi.org/10.1007/s10584-011-0155-0, 2011.

Lee, B. H., Mohr, C., Lopez-Hilfiker, F. D., Lutz, A., Hallquist, M., Lee, L., Romer, P., Cohen, R. C., Iyer, S., Kurten, T., Hu, W. W., Day, D. A., Campuzano-Jost, P., Jimenez, J. L., Xu, L., Ng, N. L., Guo, H., Weber, R. J., Wild, R. J., Brown, S. S., Koss, A., de Gouw, J., Olson, K., Goldstein, A. H., Seco, R., Kim, S., McAvey, K. M., Shepson, P. B., Starn, T., Baumann, K., Edgerton, E., Liu, J., Shilling, J. E., Miller, D. O., Brune, W. H., Schobesberger, S., D'Ambro, E. L., and Thornton, J. A.: Highly functionalized organic nitrates in the Southeast U.S.: contribution to secondary organic aerosol and reactive nitrogen budgets, Proceedings of the National Academy of Sciences, 113, 1516–1521, doi:10.1073/pnas.1508108113, 2016.

Lee, L., Teng, A. P., Wennberg, P. O., Crounse, J. D., and Cohen, R. C.: On Rates and Mechanisms of OH and O 3 Reactions with Isoprene-Derived Hydroxy Nitrates, J. Phys. Chem. A, 118, 1622–1637, doi:10.1021/jp4107603, http://dx.doi.org/10.1021/jp4107603, 2014.

Li, J., Mao, J., Pollack, I. B., Ryerson, T. B., Wolfe, G. M., Cohen, R. C., and Horowitz, L. W.: Decadal change of organic nitrates and ozone over eastern US, in preparation.

Liang, J., Horowitz, L. W., Jacob, D. J., Wang, Y., Fiore, A. M., Logan, J. A., Gardner, G. M., and Munger, J. W.: Seasonal budgets of reactive nitrogen species and ozone over the United States, and export fluxes to the global atmosphere, Journal of Geophysical Research: Atmospheres (1984–2012), 103, 13 435–13 450, 1998.

Lin, G., Penner, J. E., Sillman, S., Taraborrelli, D., and Lelieveld, J.: Global modeling of SOA formation from dicarbonyls, epoxides, organic nitrates and peroxides, Atmospheric Chemistry and Physics, 12, 4743–4774, doi:10.5194/acp-12-4743-2012, http://www.atmos-chem-phys.net/12/4743/2012/, 2012.

Liu, S., Shilling, J. E., Song, C., Hiranuma, N., Zaveri, R. A., and Russell, L. M.: Hydrolysis of Organonitrate Functional Groups in Aerosol Particles, Aerosol Science and Technology, 46, 1359–1369, doi:10.1080/02786826.2012.716175, http://dx.doi.org/10.1080/02786826.2012.716175, 2012.

Lockwood, A. L., Filley, T. R., Rhodes, D., and Shepson, P. B.: Foliar uptake of atmospheric organic nitrates, Geophysical Research Letters, 35, doi:10.1029/2008GL034714, http://dx.doi.org/10.1029/2008GL034714, 115809, 2008.

Lockwood, A. L., Shepson, P. B., Fiddler, M. N., and Alaghmand, M.: Isoprene nitrates: preparation, separation, identification, yields, and atmospheric chemistry, Atmospheric Chemistry and Physics, 10, 6169–6178, doi:10.5194/acp-10-6169-2010, http://www.atmos-chem-phys.net/10/6169/2010/, 2010.

Mao, J., Paulot, F., Jacob, D. J., Cohen, R. C., Crounse, J. D., Wennberg, P. O., Keller, C. A., Hudman, R. C., Barkley, M. P., and Horowitz, L. W.: Ozone and organic nitrates over the eastern United States: Sensitivity to isoprene chemistry, Journal of Geophysical Research: Atmospheres, 118, 11,256–11,268, doi:10.1002/jgrd.50817, http://dx.doi.org/10.1002/jgrd.50817, 2013.

Marais, E. A., Jacob, D. J., Jimenez, J. L., Campuzano-Jost, P., Day, D. A., Hu, W., Krechmer, J., Zhu, L., Kim, P. S., Miller, C. C., Fisher, J. A., Travis, K., Yu, K., Hanisco, T. F., Wolfe, G. M., Arkinson, H. L., Pye, H. O. T., Froyd, K. D., Liao, J., and McNeill, V. F.: Aqueous-

phase mechanism for secondary organic aerosol formation from isoprene: application to the Southeast United States and co-benefit of SO_2 emission controls, Atmospheric Chemistry and Physics, 16, 1603–1618, doi:10.5194/acp-16-1603-2016, 2016.

Monks, P. S., Archibald, A. T., Colette, A., Cooper, O., Coyle, M., Derwent, R., Fowler, D., Granier, C., Law, K. S., Mills, G. E., Stevenson, D. S., Tarasova, O., Thouret, V., von Schneidemesser, E., Sommariva, R., Wild, O., and Williams, M. L.: Tropospheric ozone and its precursors from the urban to the global scale from air quality to short-lived climate forcer, Atmospheric Chemistry and Physics, 15, 8889–8973, doi:10.5194/acp-15-8889-2015, http://dx.doi.org/10.5194/acp-15-8889-2015, 2015.

Müller, J.-F., Peeters, J., and Stavrakou, T.: Fast photolysis of carbonyl nitrates from isoprene, Atmospheric Chemistry and Physics, 14, 2497–2508, doi:10.5194/acp-14-2497-2014, http://www.atmos-chem-phys.net/14/2497/2014/, 2014.

Ng, N. L., Kwan, A. J., Surratt, J. D., Chan, A. W. H., Chhabra, P. S., Sorooshian, A., Pye, H. O. T., Crounse, J. D., Wennberg, P. O., Flagan, R. C., and Seinfeld, J. H.: Secondary organic aerosol (SOA) formation from reaction of isoprene with nitrate radicals (NO_3), Atmospheric Chemistry and Physics, 8, 4117–4140, doi:10.5194/acp-8-4117-2008, http://www.atmos-chem-phys.net/8/4117/2008/, 2008.

Nguyen, T. B., Crounse, J. D., Schwantes, R. H., Teng, A. P., Bates, K. H., Zhang, X., St. Clair, J. M., Brune, W. H., Tyndall, G. S., Keutsch, F. N., Seinfeld, J. H., and Wennberg, P. O.: Overview of the Focused Isoprene eXperiment at the California Institute of Technology (FIXCIT): mechanistic chamber studies on the oxidation of biogenic compounds, Atmospheric Chemistry and Physics, 14, 13 531–13 549, doi:10.5194/acp-14-13531-2014, http://www.atmos-chem-phys.net/14/13531/2014/, 2014.

Nguyen, T. B., Crounse, J. D., Teng, A. P., Clair, J. M. S., Paulot, F., Wolfe, G. M., and Wennberg, P. O.: Rapid deposition of oxidized biogenic compounds to a temperate forest, Proceedings of the National Academy of Sciences, 112, E392–E401, doi:10.1073/pnas.1418702112, http://dx.doi.org/10.1073/pnas.1418702112, 2015.

Nozière, B., Barnes, I., and Becker, K.-H.: Product study and mechanisms of the reactions of α-pinene and of pinonaldehyde with OH radicals, Journal of Geophysical Research: Atmospheres (1984–2012), 104, 23 645–23 656, 1999.

O'Brien, J., Shepson, P., Muthuramu, K., Hao, C., Niki, H., Hastie, D., Taylor, R., and Roussel, P.: Measurements of alkyl and multifunctional organic nitrates at a rural site in Ontario, Journal of Geophysical Research, 1995.

Palmer, P. I., Abbot, D. S., Fu, T.-M., Jacob, D. J., Chance, K., Kurosu, T. P., Guenther, A., Wiedinmyer, C., Stanton, J. C., Pilling, M. J., Pressley, S. N., Lamb, B., and Sumner, A. L.: Quantifying the seasonal and interannual variability of North American isoprene emissions using satellite observations of the formaldehyde column, J. Geophys. Res., 111, doi:10.1029/2005jd006689, http://dx.doi.org/10.1029/2005JD006689, 2006.

Patchen, A. K., Pennino, M. J., Kiep, A. C., and Elrod, M. J.: Direct kinetics study of the product-forming channels of the reaction of isoprene-derived hydroxyperoxy radicals with NO, International Journal of Chemical Kinetics, 39, 353–361, doi:10.1002/kin.20248, http://dx.doi.org/10.1002/kin.20248, 2007.

Paulot, F., Crounse, J. D., Kjaergaard, H. G., Kroll, J. H., Seinfeld, J. H., and Wennberg, P. O.: Isoprene photooxidation: new insights into the production of acids and organic nitrates, Atmospheric Chemistry and Physics, 9, 1479–1501, doi:10.5194/acp-9-1479-2009, http://www.atmos-chem-phys.net/9/1479/2009/, 2009.

Paulot, F., Henze, D. K., and Wennberg, P. O.: Impact of the isoprene photochemical cascade on tropical ozone, Atmospheric Chemistry and Physics, 12, 1307–1325, doi:10.5194/acp-12-1307-2012, http://dx.doi.org/10.5194/acp-12-1307-2012, 2012.

Peeters, J., Müller, J.-F., Stavrakou, T., and Nguyen, V. S.: Hydroxyl Radical Recycling in Isoprene Oxidation Driven by Hydrogen Bonding and Hydrogen Tunneling: The Upgraded LIM1 Mechanism, J. Phys. Chem. A, 118, 8625–8643, doi:10.1021/jp5033146, http://dx.doi.org/10.1021/jp5033146, 2014.

Perring, A. E., Bertram, T. H., Wooldridge, P. J., Fried, A., Heikes, B. G., Dibb, J., Crounse, J. D., Wennberg, P. O., Blake, N. J., Blake, D. R., Brune, W. H., Singh, H. B., and Cohen, R. C.: Airborne observations of total $RONO_2$: new constraints on the yield and lifetime of isoprene nitrates, Atmospheric Chemistry and Physics, 9, 1451–1463, doi:10.5194/acp-9-1451-2009, http://www.atmos-chem-phys.net/9/1451/2009/, 2009a.

5   Perring, A. E., Wisthaler, A., Graus, M., Wooldridge, P. J., Lockwood, A. L., Mielke, L. H., Shepson, P. B., Hansel, A., and Cohen, R. C.: A product study of the isoprene+NO_3 reaction, Atmospheric Chemistry and Physics, 9, 4945–4956, doi:10.5194/acp-9-4945-2009, http://www.atmos-chem-phys.net/9/4945/2009/, 2009b.

Perring, A. E., Pusede, S. E., and Cohen, R. C.: An Observational Perspective on the Atmospheric Impacts of Alkyl and Multifunctional Nitrates on Ozone and Secondary Organic Aerosol, Chemical Reviews, 113, 5848–5870, doi:10.1021/cr300520x, http://dx.doi.org/10.1021/cr300520x, 2013.

Pye, H. O. T., Luecken, D. J., Xu, L., Boyd, C. M., Ng, N. L., Baker, K. R., Ayres, B. R., Bash, J. O., Baumann, K., Carter, W. P. L., Edgerton, E., Fry, J. L., Hutzell, W. T., Schwede, D. B., and Shepson, P. B.: Modeling the Current and Future Roles of Particulate Organic Nitrates in the Southeastern United States, Environmental Science & Technology, doi:10.1021/acs.est.5b03738, http://dx.doi.org/10.1021/acs.est.5b03738, 2015.

15   Rindelaub, J. D., McAvey, K. M., and Shepson, P. B.: The photochemical production of organic nitrates from α-pinene and loss via acid-dependent particle phase hydrolysis, Atmospheric Environment, 100, 193–201, doi:10.1016/j.atmosenv.2014.11.010, http://dx.doi.org/10.1016/j.atmosenv.2014.11.010, 2015.

Roberts, J. M. and Fajer, R. W.: UV absorption cross sections of organic nitrates of potential atmospheric importance and estimation of atmospheric lifetimes, Environmental science & technology, 23, 945–951, 1989.

20   Rollins, A. W., Kiendler-Scharr, A., Fry, J. L., Brauers, T., Brown, S. S., Dorn, H.-P., Dubé, W. P., Fuchs, H., Mensah, A., Mentel, T. F., Rohrer, F., Tillmann, R., Wegener, R., Wooldridge, P. J., and Cohen, R. C.: Isoprene oxidation by nitrate radical: alkyl nitrate and secondary organic aerosol yields, Atmospheric Chemistry and Physics, 9, 6685–6703, doi:10.5194/acp-9-6685-2009, http://www.atmos-chem-phys.net/9/6685/2009/, 2009.

Rollins, A. W., Smith, J. D., Wilson, K. R., and Cohen, R. C.: Real Time In Situ Detection of Organic Nitrates in Atmospheric Aerosols, Environmental Science & Technology, 44, 5540–5545, doi:10.1021/es100926x, http://dx.doi.org/10.1021/es100926x, pMID: 20575535, 2010.

Rollins, A. W., Browne, E. C., Min, K.-E., Pusede, S. E., Wooldridge, P. J., Gentner, D. R., Goldstein, A. H., Liu, S., Day, D. A., Russell, L. M., and Cohen, R. C.: Evidence for NOx Control over Nighttime SOA Formation, Science, 337, 1210–1212, doi:10.1126/science.1221520, http://dx.doi.org/10.1126/science.1221520, 2012.

30   Rollins, A. W., Pusede, S., Wooldridge, P., Min, K.-E., Gentner, D. R., Goldstein, A. H., Liu, S., Day, D. A., Russell, L. M., Rubitschun, C. L., Surratt, J. D., and Cohen, R. C.: Gas/particle partitioning of total alkyl nitrates observed with TD-LIF in Bakersfield, Journal of Geophysical Research: Atmospheres, 118, 6651–6662, doi:10.1002/jgrd.50522, http://dx.doi.org/10.1002/jgrd.50522, 2013.

Romer, P. S., Duffey, K. C., Wooldridge, P. J., Allen, H. M., Ayres, B. R., Brown, S. S., Brune, W. H., Crounse, J. D., de Gouw, J., Draper, D. C., Feiner, P. A., Fry, J. L., Goldstein, A. H., Koss, A., Misztal, P. K., Nguyen, T. B., Olson, K., Teng, A. P., Wennberg, P. O., Wild, R. J.,

35   Zhang, L., and Cohen, R. C.: The Lifetime of Nitrogen Oxides in an Isoprene Dominated Forest, Atmospheric Chemistry and Physics Discussions, 2016, 1–25, doi:10.5194/acp-2016-28, http://www.atmos-chem-phys-discuss.net/acp-2016-28/, 2016.

Schwantes, R. H., Teng, A. P., Nguyen, T. B., Coggon, M. M., Crounse, J. D., Clair, J. M. S., Zhang, X., Schilling, K. A., Seinfeld, J. H., and Wennberg, P. O.: Isoprene NO3 Oxidation Products from the RO2 + HO2 Pathway, The Journal of Physical Chemistry A, 119, 10 158–10 171, doi:10.1021/acs.jpca.5b06355, http://dx.doi.org/10.1021/acs.jpca.5b06355, pMID: 26335780, 2015.

Simon, H., Reff, A., Wells, B., Xing, J., and Frank, N.: Ozone Trends Across the United States over a Period of Decreasing NOx and VOC Emissions, Environmental Science & Technology, 49, 186–195, doi:10.1021/es504514z, http://dx.doi.org/10.1021/es504514z, 2015.

Singh, H. B. and Hanst, P. L.: Peroxyacetyl nitrate (PAN) in the unpolluted atmosphere: An important reservoir for nitrogen oxides, Geophysical Research Letters, 8, 941–944, doi:10.1029/GL008i008p00941, http://dx.doi.org/10.1029/GL008i008p00941, 1981.

Sprengnether, M., Demerjian, K. L., Donahue, N. M., and Anderson, J. G.: Product analysis of the OH oxidation of isoprene and 1,3-butadiene in the presence of NO, Journal of Geophysical Research: Atmospheres, 107, ACH 8–1–ACH 8–13, doi:10.1029/2001JD000716, http://dx.doi.org/10.1029/2001JD000716, 2002.

Talukdar, R. K., Burkholder, J. B., Hunter, M., Gilles, M. K., Roberts, J. M., and Ravishankara, A. R.: Atmospheric fate of several alkyl nitrates Part 2UV absorption cross-sections and photodissociation quantum yields, J. Chem. Soc., Faraday Trans., 93, 2797–2805, doi:10.1039/A701781B, http://dx.doi.org/10.1039/A701781B, 1997.

Teng, A. P., Crounse, J. D., and Wennberg, P. O.: Isoprene peroxy radical dynamics, in preparation.

Toon, O. B., Maring, H., Dibb, J., Ferrare, R., Jacob, D. J., Jensen, E. J., Luo, Z. J., Mace, G. G., Pan, L. L., Pfister, L., Rosenlof, K. H., Redemann, J., Reid, J. S., Singh, H. B., Yokelson, R., Minnis, P., Chen, G., Jucks, K. W., and Pszenny, A.: Planning, implementation and scientific goals of the Studies of Emissions and Atmospheric Composition, Clouds and Climate Coupling by Regional Surveys (SEAC4RS) field mission, Journal of Geophysical Research, accepted manuscript, doi:10.1002/2015JD024297, 2016.

Travis, K. R., Jacob, D. J., Fisher, J. A., Kim, P. S., Marais, E. A., Zhu, L., Yu, K., Miller, C. C., Yantosca, R. M., Sulprizio, M. P., Thompson, A. M., Wennberg, P. O., Crounse, J. D., St. Clair, J. M., Cohen, R. C., Laughner, J. L., Dibb, J. E., Hall, S. R., Ullmann, K., Wolfe, G. M., Neuman, J. A., and Zhou, X.: NOx emissions, isoprene oxidation pathways, vertical mixing, and implications for surface ozone in the Southeast United States, in review for Atmospheric Chemistry and Physics, doi:10.5194/acp-2016-110, 2016.

Tuazon, E. C. and Atkinson, R.: A product study of the gas-phase reaction of Isoprene with the OH radical in the presence of NOx, International Journal of Chemical Kinetics, 22, 1221–1236, doi:10.1002/kin.550221202, http://dx.doi.org/10.1002/kin.550221202, 1990.

Wainwright, C. D., Pierce, J. R., Liggio, J., Strawbridge, K. B., Macdonald, A. M., and Leaitch, R. W.: The effect of model spatial resolution on Secondary Organic Aerosol predictions: a case study at Whistler, BC, Canada, Atmospheric Chemistry and Physics, 12, 10 911–10 923, doi:10.5194/acp-12-10911-2012, http://www.atmos-chem-phys.net/12/10911/2012/, 2012.

Wang, Y. X., McElroy, M. B., Jacob, D. J., and Yantosca, R. M.: A nested grid formulation for chemical transport over Asia: Applications to CO, Journal of Geophysical Research: Atmospheres, 109, n/a–n/a, doi:10.1029/2004JD005237, http://dx.doi.org/10.1029/2004JD005237, d22307, 2004.

Wolfe, G. M., Hanisco, T. F., Arkinson, H. L., Bui, T. P., Crounse, J. D., Dean-Day, J., Goldstein, A., Guenther, A., Hall, S. R., Huey, G., Jacob, D. J., Karl, T., Kim, P. S., Liu, X., Marvin, M. R., Mikoviny, T., Misztal, P. K., Nguyen, T. B., Peischl, J., Pollack, I., Ryerson, T., St. Clair, J. M., Teng, A., Travis, K. R., Ullmann, K., Wennberg, P. O., and Wisthaler, A.: Quantifying sources and sinks of reactive gases in the lower atmosphere using airborne flux observations, Geophysical Research Letters, 42, 8231–8240, doi:10.1002/2015GL065839, http://dx.doi.org/10.1002/2015GL065839, 2015GL065839, 2015.

Worton, D. R., Reeves, C. E., Penkett, S. A., Sturges, W. T., Slemr, J., Oram, D. E., Bandy, B. J., Bloss, W. J., Carslaw, N., Davey, J., Emmerson, K. M., Gravestock, T. J., Hamilton, J. F., Heard, D. E., Hopkins, J. R., Hulse, A., Ingram, T., Jacob, M. J., Lee, J. D., Leigh, R. J., Lewis, A. C., Monks, P. S., and Smith, S. C.: Alkyl nitrate photochemistry during the tropospheric organic chemistry experiment,

Atmospheric Environment, 44, 773 – 785, doi:http://dx.doi.org/10.1016/j.atmosenv.2009.11.038, http://www.sciencedirect.com/science/article/pii/S1352231009009923, 2010.

Xie, Y., Paulot, F., Carter, W. P. L., Nolte, C. G., Luecken, D. J., Hutzell, W. T., Wennberg, P. O., Cohen, R. C., and Pinder, R. W.: Understanding the impact of recent advances in isoprene photooxidation on simulations of regional air quality, Atmospheric Chemistry and Physics, 13, 8439–8455, doi:10.5194/acp-13-8439-2013, http://www.atmos-chem-phys.net/13/8439/2013/, 2013.

Xiong, F., McAvey, K. M., Pratt, K. A., Groff, C. J., Hostetler, M. A., Lipton, M. A., Starn, T. K., Seeley, J. V., Bertman, S. B., Teng, A. P., Crounse, J. D., Nguyen, T. B., Wennberg, P. O., Misztal, P. K., Goldstein, A. H., Guenther, A. B., Koss, A. R., Olson, K. F., de Gouw, J. A., Baumann, K., Edgerton, E. S., Feiner, P. A., Zhang, L., Miller, D. O., Brune, W. H., and Shepson, P. B.: Observation of isoprene hydroxynitrates in the southeastern United States and implications for the fate of NO_x, Atmospheric Chemistry and Physics, 15, 11 257–11 272, doi:10.5194/acp-15-11257-2015, http://www.atmos-chem-phys.net/15/11257/2015/, 2015.

Xu, L., Guo, H., Boyd, C. M., Klein, M., Bougiatioti, A., Cerully, K. M., Hite, J. R., Isaacman-VanWertz, G., Kreisberg, N. M., Knote, C., Olson, K., Koss, A., Goldstein, A. H., Hering, S. V., de Gouw, J., Baumann, K., Lee, S.-H., Nenes, A., Weber, R. J., and Ng, N. L.: Effects of anthropogenic emissions on aerosol formation from isoprene and monoterpenes in the southeastern United States, Proceedings of the National Academy of Sciences, 112, 37–42, doi:10.1073/pnas.1417609112, http://dx.doi.org/10.1073/pnas.1417609112, 2014.

Xu, L., Suresh, S., Guo, H., Weber, R. J., and Ng, N. L.: Aerosol characterization over the southeastern United States using high-resolution aerosol mass spectrometry: spatial and seasonal variation of aerosol composition and sources with a focus on organic nitrates, Atmospheric Chemistry and Physics, 15, 7307–7336, doi:10.5194/acp-15-7307-2015, http://dx.doi.org/10.5194/acp-15-7307-2015, 2015.

Yu, K., Jacob, D. J., Fisher, J. A., Kim, P. S., Marais, E. A., Miller, C. C., Travis, K. R., Zhu, L., Yantosca, R. M., Sulprizio, M. P., Cohen, R. C., Dibb, J. E., Fried, A., Mikoviny, T., Ryerson, T. B., Wennberg, P. O., and Wisthaler, A.: Sensitivity to grid resolution in the ability of a chemical transport model to simulate observed oxidant chemistry under high-isoprene conditions, Atmospheric Chemistry and Physics, 16, doi:10.5194/acp-16-4369-2016, 2016.

Zhang, L., Jacob, D. J., Downey, N. V., Wood, D. A., Blewitt, D., Carouge, C. C., van Donkelaar, A., Jones, D. B., Murray, L. T., and Wang, Y.: Improved estimate of the policy-relevant background ozone in the United States using the GEOS-Chem global model with $1/2\,^{\circ} \times 2/3\,^{\circ}$ horizontal resolution over North America, Atmospheric Environment, 45, 6769 – 6776, doi:http://dx.doi.org/10.1016/j.atmosenv.2011.07.054, http://www.sciencedirect.com/science/article/pii/S1352231011007989, 2011.

Zhang, L., Jacob, D. J., Knipping, E. M., Kumar, N., Munger, J. W., Carouge, C. C., van Donkelaar, A., Wang, Y. X., and Chen, D.: Nitrogen deposition to the United States: distribution, sources, and processes, Atmospheric Chemistry and Physics, 12, 4539–4554, doi:10.5194/acp-12-4539-2012, http://www.atmos-chem-phys.net/12/4539/2012/, 2012.

Zhu, L., Jacob, D. J., Kim, P. S., Fisher, J. A., Yu, K., Travis, K. R., Mickley, L. J., Yantosca, R. M., Sulprizio, M. P., De Smedt, I., Gonzalez Abad, G., Chance, K., Li, C., Ferrare, R., Fried, A., Hair, J. W., Hanisco, T. F., , Richter, D., Scarino, A. J., Walega, J., Weibring, P., and Wolfe, G. M.: Observing atmospheric formaldehyde (HCHO) from space: validation and intercomparison of six retrievals from four satellites (OMI, GOME2A, GOME2B, OMPS) with SEAC4RS aircraft observations over the Southeast US, in review for Atmospheric Chemistry and Physics, doi:10.5194/acp-2016-162, 2016.
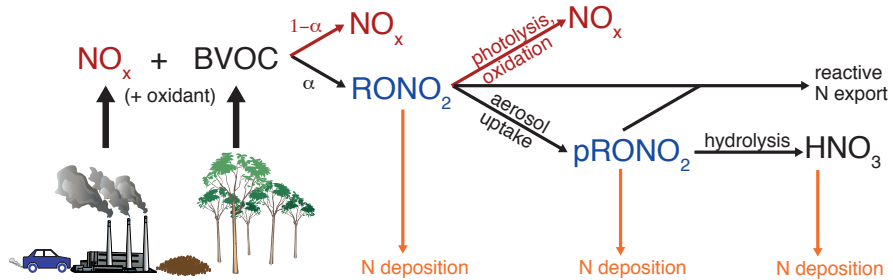
Figure 1. Schematic representation of organic nitrate chemistry and impacts. Organic nitrates are shown in blue, NO_x and processes that recycle NO_x are shown in red, and nitrogen deposition is shown in orange. Symbols courtesy of the Integration and Application Network, University of Maryland Center for Environmental Science (ian.umces.edu/symbols/).
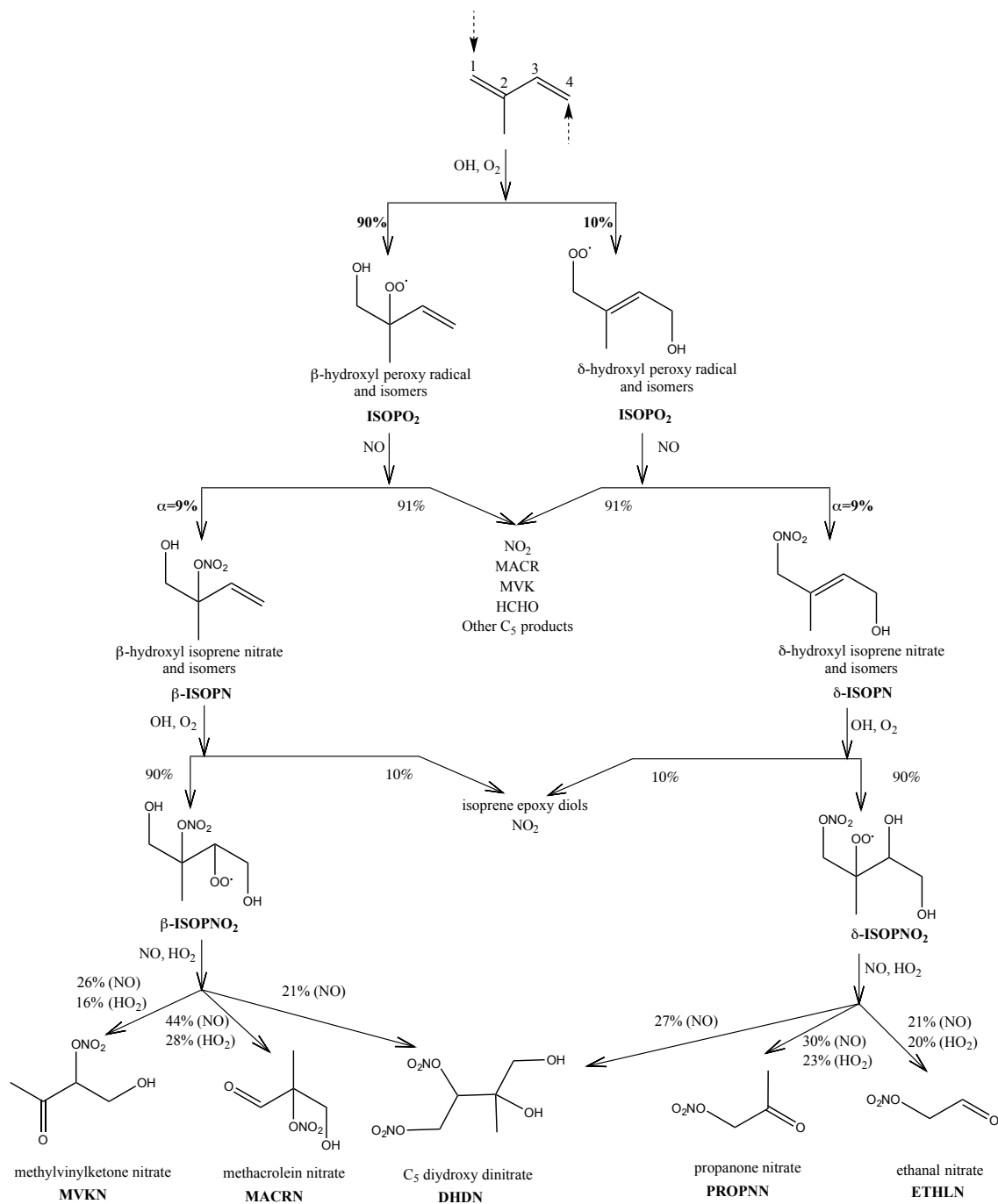
Figure 2. Schematic of the formation of isoprene nitrates (INs) from OH-initiated isoprene oxidation as implemented in GEOS-Chem. The isomers shown are indicative as the mechanism does not distinguish between isomers (except for β- vs. δ-configurations). For ISOPNO$_2$ oxidation, only IN products are shown, along with their yields from both NO and HO$_2$ pathways. Small yields (<10%) of MVKN and MACRN from δ-ISOPNO$_2$ are not shown.
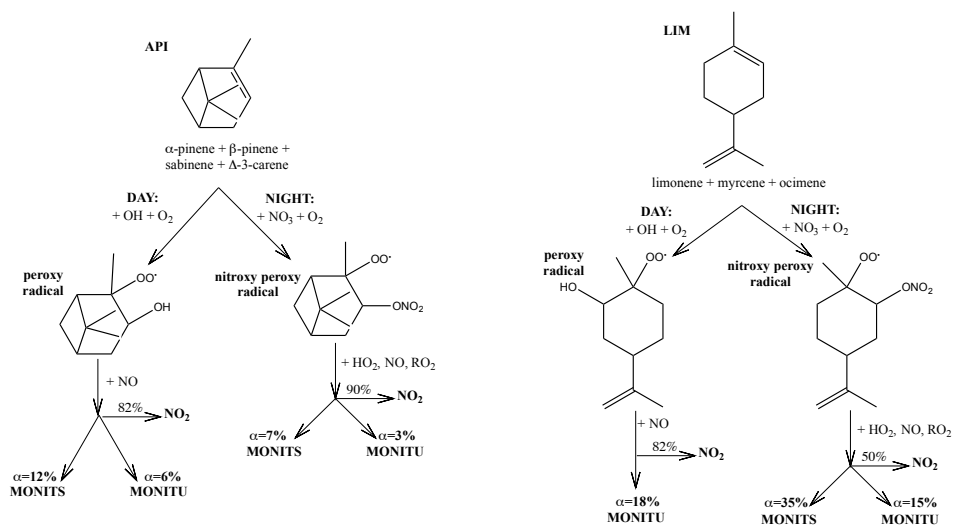
Figure 3. Simplified representation of the formation of monoterpene nitrates (MTN) from monoterpene oxidation as implemented in GEOS-Chem. For each lumped species, only one indicative form is shown.
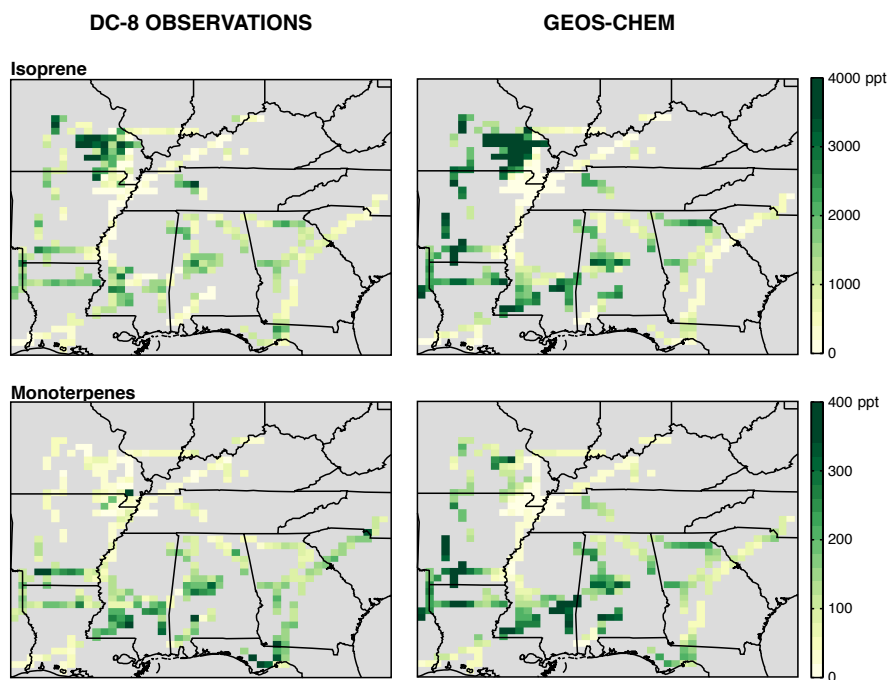
Figure 4. Observed (left) and simulated (right) mixing ratios of isoprene and monoterpenes below 1 km during the SEAC[4]RS aircraft campaign (12 Aug - 23 Sep 2013). The GEOS-Chem model has been sampled along the aircraft flight tracks, and the observations binned to the spatial and temporal resolution of the model. The normalized mean bias of the simulation relative to the PTR-MS measurements in the lowest 500 m is +34% for isoprene and +3% for monoterpenes.
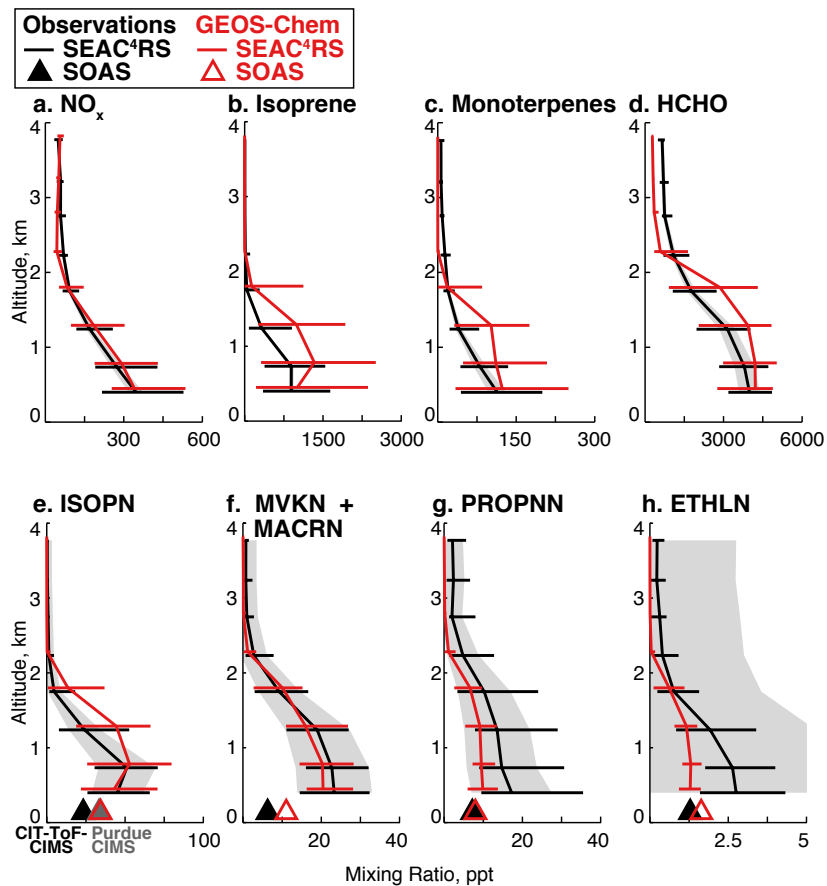
Figure 5. Observed (black) and modeled (red) median 0-4 km profiles of NO_x, biogenic VOCs, and oxidation products over the Southeast US (80-94.5°W, 29.5-40°N) during $SEAC^4RS$. Data are binned in 500m increments, and horizontal lines indicate the interquartile range within each bin. Gray shading represents the measurement uncertainty. The model has been sampled in the same manner as the observations, as described in the text. For organic nitrates (e-h), SOAS campaign median surface values are shown as triangles. For ISOPN (e), the gray triangle represents the Purdue CIMS and the black triangle the CIT-ToF-CIMS.
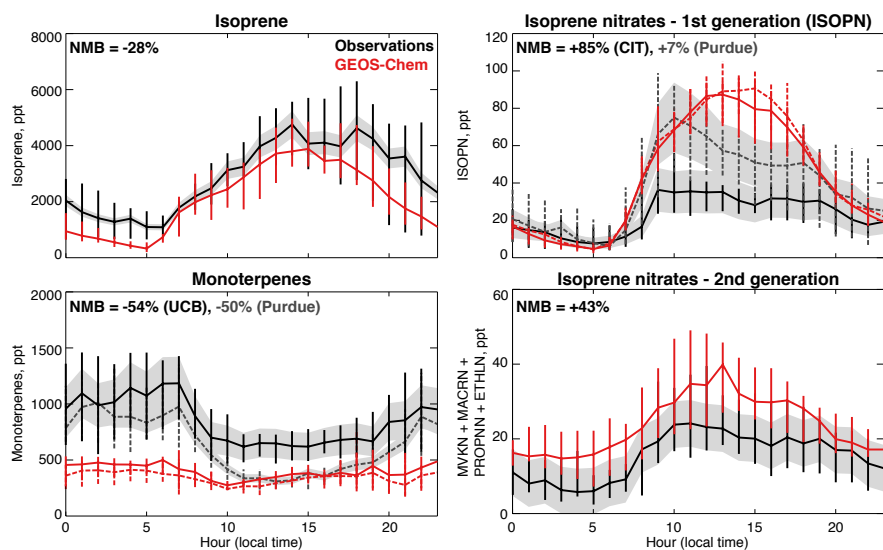
Figure 6. Observed (black, gray) and simulated (red) median diurnal cycles of isoprene, monoterpenes, first generation isoprene nitrates (ISOPN), and second generation isoprene nitrates (MVKN+MACRN+PROPNN+ETHLN) at Centreville during the 2013 SOAS campaign. Gray shading represents the measurement uncertainty, vertical bars show the interquartile range of the hourly data, and the normalized mean bias (NMB) of the simulation is given inset. The model has been sampled in the Centreville grid box only for hours with available data during 16 June - 11 July for isoprene and monoterpenes from the UC Berkeley PTR-ToF-MS (solid black), 13 June - 15 July for α-pinene + β-pinene from the Purdue 2D-GF-FID (dashed gray), 1 June - 11 July for ISOPN from the Purdue CIMS (dashed gray), and 1 June - 4 July for ISOPN and 2nd generation isoprene nitrates from the CIT-ToF-CIMS (solid black). For ISOPN and monoterpenes, differences in data availability between the two measurements result in slightly different model values (solid/dashed red lines).
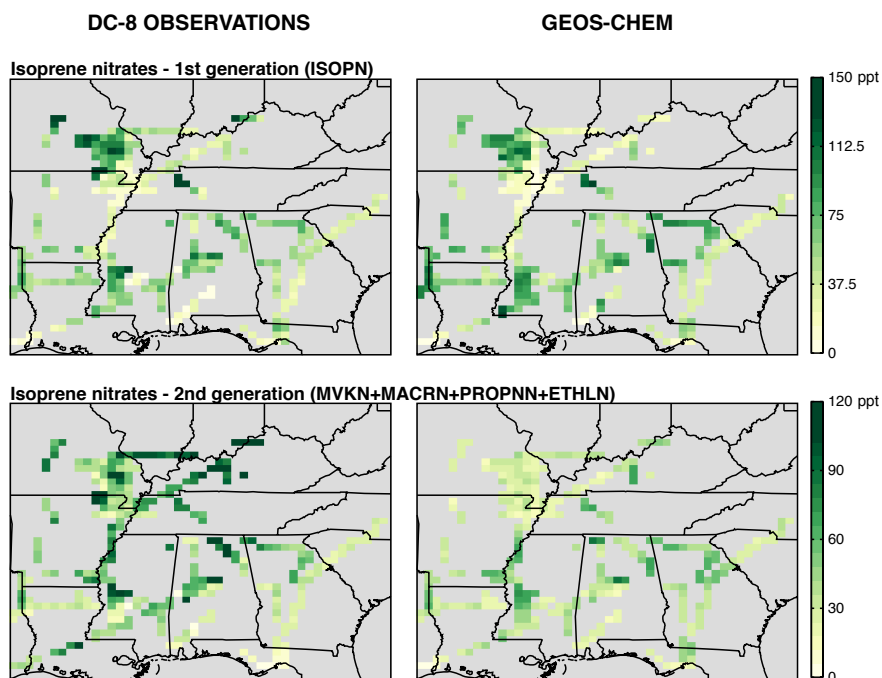
Figure 7. Observed (left) and simulated (right) mixing ratios of isoprene nitrates below 1 km during SEAC[4]RS, separated into first generation (ISOPN) and second generation (MVKN+MACRN+PROPNN+ETHLN) species. The GEOS-Chem simulation has been sampled along the aircraft flight tracks, and the observations binned to the spatial and temporal resolution of the model, as described in the text. The normalized mean bias of the simulation relative to the measurements in the lowest 500 m is -0.6% for ISOPN and -35% for second generation isoprene nitrates.
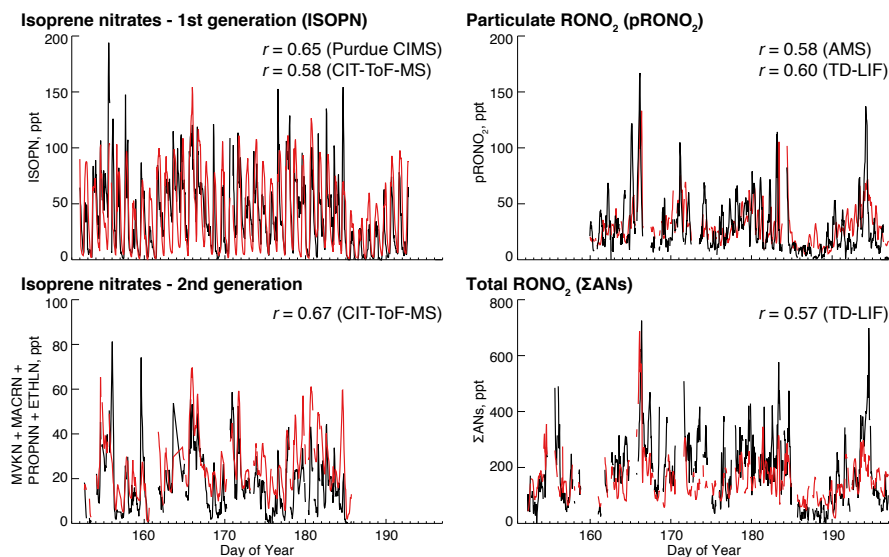
Figure 8. Timeseries of observed (black) and simulated (red) hourly mean $RONO_2$ at Centreville during the 2013 SOAS campaign for 1st generation isoprene nitrates (ISOPN, from the Purdue CIMS), 2nd generation isoprene nitrates (MVKN+MACRN+PROPNN+ETHLN from the CIT-ToF-CIMS), particulate $RONO_2$ ($pRONO_2$, from the AMS) and total alkyl nitrates (ΣANs, from the TD-LIF). The model has been sampled in the Centreville grid box only for hours with available data from each instrument. The model-observation correlation coefficient (r) for each species is given inset both for the measurement shown and (where available) for additional measurement of the same species (with timeseries shown in Fig. S4).
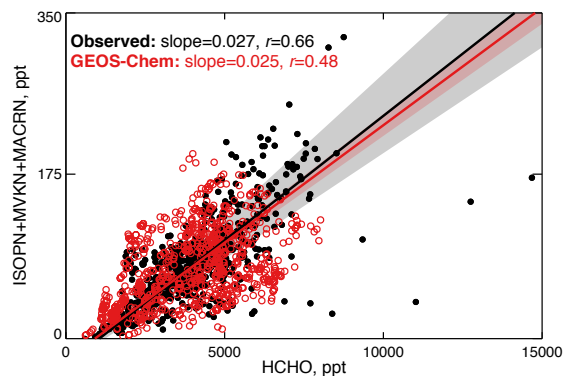
Figure 9. Observed (black) and simulated (red) correlations between HCHO and the sum of major isoprene nitrates produced via daytime isoprene oxidation (ISOPN+MVKN+MACRN) in Southeast US surface air (<1 km) during SEAC[4]RS. Thick solid lines indicate the best fit as calculated from a reduced major axis regression, and shaded areas show the 95% confidence interval on the regression slope as determined by bootstrap resampling. The regression slopes and correlation coefficients are given inset.
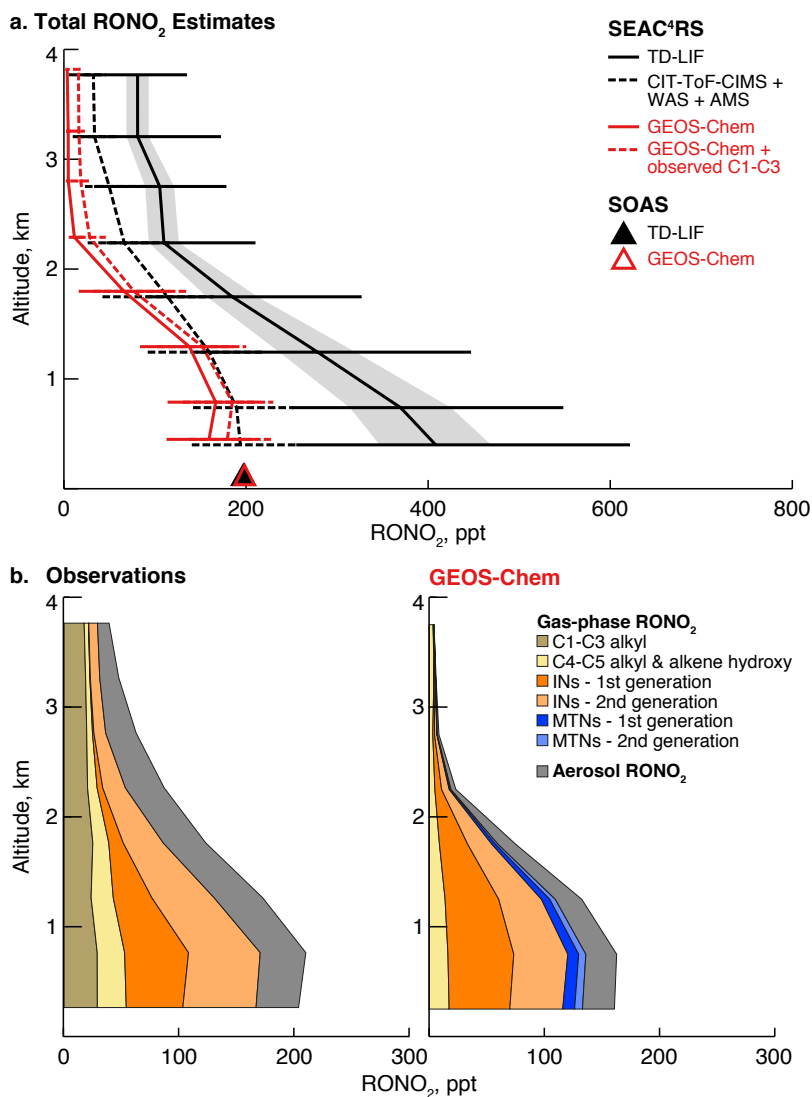
Figure 10. (a) Median vertical profiles of estimated total $RONO_2$ over the Southeast US during SEAC⁴RS. For the observations, the solid black line indicates the TD-LIF ΣANs measurements (with gray shading for the measurement uncertainty) and the dashed black line the sum of CIT-ToF-CIMS, WAS, and AMS measurements of individual $RONO_2$ species (gas-phase and particulate). For the model, the solid red line indicates the total simulated $RONO_2$ and the dashed red line the sum of total simulated $RONO_2$ plus measured ≤C_3 RONO2 that are not included in the simulation. Triangles compare the total $RONO_2$ during SOAS from TD-LIF ΣANs and GEOS-Chem. (b) Mean $RONO_2$ composition from the observations (CIT-ToF-CIMS, WAS, and AMS) and the model. Isoprene nitrates (INs) include 1st generation (ISOPN, plus ISN1 for GEOS-Chem) and 2nd generation INs (MVKN+MACRN, PROPNN, ETHLN, NISOPOOH, plus DHDN for GEOS-Chem). Monoterpene nitrates (MTNs) are shown for the model only and include first and second generation contributions. Other gas-phase $RONO_2$ (yellow, brown) are mainly anthropogenic and do not represent the same species between the model and the observations.
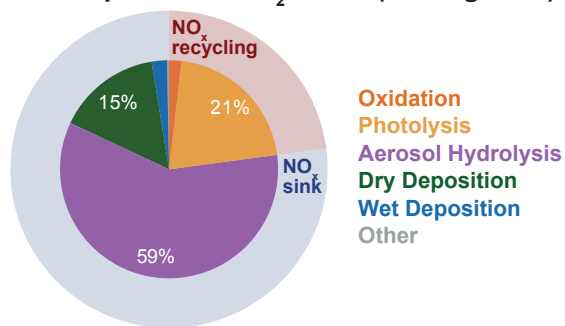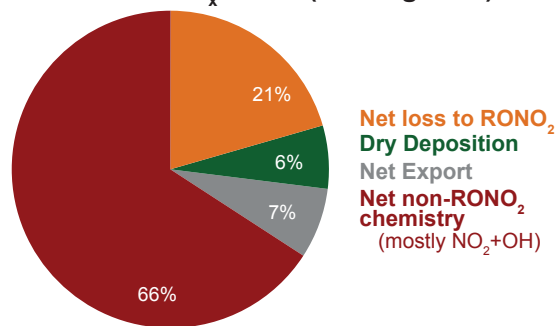
Figure 11. Simulated relative importance of gas-phase loss processes (%) in the Southeast US boundary layer (80-94.5°W, 29.5-40°N, <2 km) during August-September 2013 for (a) gas-phase $RONO_2$ and (b) NO_x. In (a), outer circles group losses into those that recycle NO_x (pale red) and those that serve as terminal NO_x sinks (pale blue). Loss processes that recycle $RONO_2$ by converting between $RONO_2$ species (e.g. first to second generation) are not included. In (b), net loss to $RONO_2$ is calculated as the difference between NO_x consumed during $RONO_2$ production and NO_x recycled during $RONO_2$ loss, with recycling efficiencies from (a). Net non-$RONO_2$ chemistry is the difference between NO_x chemical production and chemical loss excluding all $RONO_2$ chemistry, and net export is the difference between emissions and all other sinks. Absolute loss rates from all processes combined (Mg N d^{-1}) are given in the sub-plot titles.
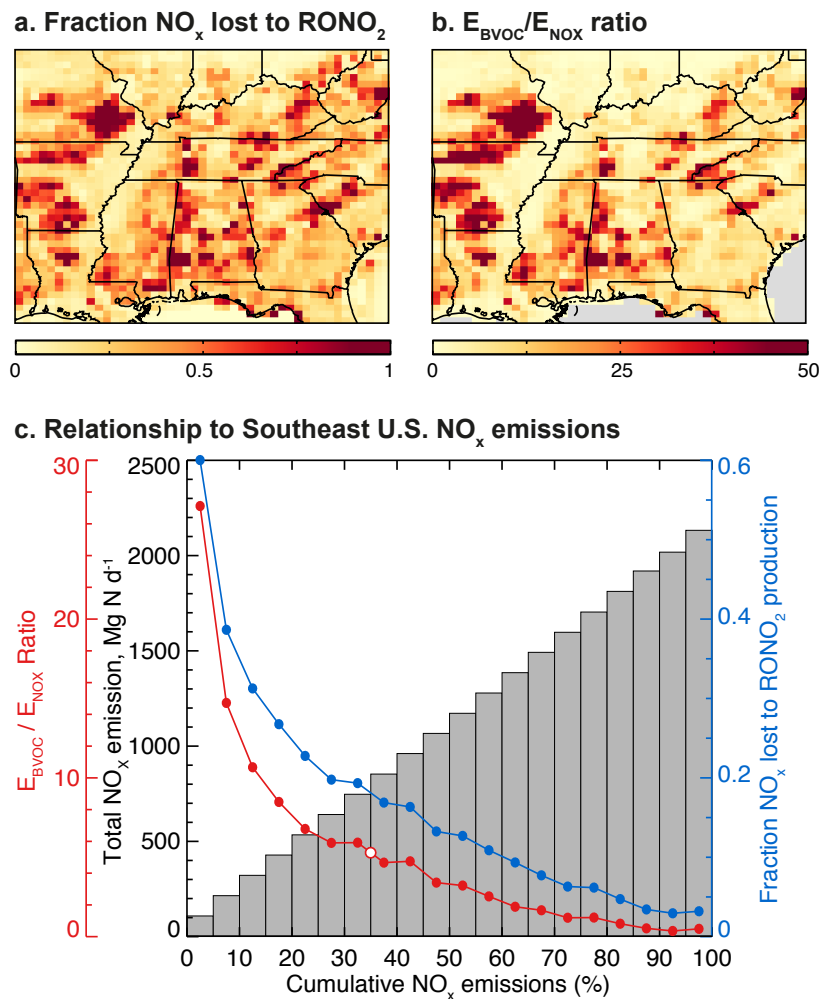
Figure 12. Importance of organic nitrates as a sink for NO_x, as a function of BVOC and NO_x emissions. (a) Simulated fraction of emitted NO_x that is lost to $RONO_2$ production in Southeast US surface air. (b) Ratio of BVOC (isoprene + monoterpene) emissions (E_{BVOC}) to NO_x emissions (E_{NOx}). (c) Mean values of variables from (a) and (b) as a function of cumulative NO_x emissions in the Southeast US. Model grid squares have been sorted by NO_x emissions then grouped into bins that each represent 5% of total Southeast US NO_x emissions. Values shown for the fractional NO_x sink due to $RONO_2$ production (blue) and the mean E_{BVOC}/E_{NOx} emissions ratio (red) represent the mean within each bin. NO_x emissions are shown as cumulative totals (gray) in Mg N day^{-1}. The Southeast US mean E_{BVOC}/E_{NOx} emissions ratio (5.3) is highlighted with a white circle.

Table 1. Gas-phase organic nitrates in GEOS-Chem: formation and loss pathways and lifetimes.[a]

Species	Model name	Principal formation pathways[b]	Removal Processes[c]	Lifetime (h)[d]
β-hydroxy isoprene nitrate	ISOPNB	ISOP + OH	aerosol hydrolysis deposition oxidation photolysis	1.8
δ-hydroxy isoprene nitrate	ISOPND	ISOP + OH	deposition oxidation aerosol hydrolysis photolysis	4.0
C_5 nitrooxy carbonyl	ISN1	ISOP + NO_3	deposition photolysis oxidation aerosol hydrolysis	0.29
C_5 nitrooxy hydroperoxide[e]	INPN	ISOP + NO_3	n/a	n/a
methyl vinyl ketone nitrate	MVKN	ISOPNB + OH	deposition aerosol hydrolysis photolysis oxidation	3.1
methacrolein nitrate	MACRN	ISOPNB + OH	photolysis deposition aerosol hydrolysis oxidation	1.5
propanone nitrate	PROPNN	ISOPND + OH ISN1 + NO_3	deposition photolysis oxidation	3.3
ethanal nitrate	ETHLN	ISOPND + OH	deposition photolysis oxidation	1.5
C_5 dihydroxy dinitrate	DHDN	ISOPND + OH ISOPND + OH	aerosol hydrolysis deposition	4.6
saturated first generation monoterpene nitrate	MONITS	API + OH API + NO_3 LIM + NO_3	deposition aerosol hydrolysis oxidation photolysis	1.8
unsaturated first generation monoterpene nitrate	MONITU	API + OH API + NO_3 LIM + OH LIM + NO_3	oxidation deposition aerosol hydrolysis photolysis	0.85
second generation monoterpene nitrate	HONIT	MONITU + OH MONITS + OH	aerosol hydrolysis deposition photolysis oxidation	1.7

[a] Model results are averaged over Southeast US surface air sampled along the SEAC[4]RS flight tracks.
[b] Primary precursor(s) and associated oxidant(s). The related peroxy radicals and their oxidants can be seen in Figs. 1 and 2.
[c] Removal processes for each species are ordered by their contribution to total loss during SEAC[4]RS. Losses due to oxidation, photolysis, and aerosol uptake are calculated along the SEAC[4]RS flight tracks. Deposition includes both dry and wet scavenging and is calculated from regional means over all Southeast US grid boxes. Wet deposition in the model is calculated for lumped species ISOPNB+ISOPND, MVKN+MACRN, and MONITU+MONITS and individually for all others. For this table, we assume partitioning of 90% ISOPNB (10% ISOPND) based on the initial formation yields and a 50:50 split for the other lumped species. Wet scavenging is only a small contribution to total $RONO_2$ deposition, and this assumption has minimal impact on these values.
[d] Lifetimes are the combined lifetimes against deposition as calculated over all grid boxes and against oxidation, photolysis, and aerosol hydrolysis as calculated along the flight tracks, with further details in note c. These are representative of daytime conditions only, as determined by the timing of the SEAC[4]RS flights.
[e] INPN is not treated as a transported species, so diagnostics needed to calculate removal rates and lifetime are not available.